Structure and Dynamics of a Proton Wire: A Theoretical Study of H^+ Translocation along the Single-File Water Chain in the Gramicidin A Channel

Régis Pomès and Benoît Roux
Groupe de Recherche en Transport Membranaire, Départements de Physique et de Chimie, Université de Montréal, Montréal, Québec H3C 3J7 Canada

ABSTRACT The rapid translocation of H^+ along a chain of hydrogen-bonded water molecules, or proton wire, is thought to be an important mechanism for proton permeation through transmembrane channels. Computer simulations are used to study the properties of the proton wire formed by the single-file waters in the gramicidin A channel. The model includes the polypeptidic dimer, with 22 water molecules and one excess proton. The dissociation of the water molecules is taken into account by the "polarization model" of Stillinger and co-workers. The importance of quantum effects due to the light mass of the hydrogen nuclei is examined with the use of discretized Feynman path integral molecular dynamics simulations. Results show that the presence of an excess proton in the pore orients the single-file water molecules and affects the geometry of water-water hydrogen bonding interactions. Rather than a well-defined hydronium ion OH_3^+ in the single-file region, the protonated species is characterized by a strong hydrogen bond resembling that of $O_2H_5^+$. The quantum dispersion of protons has a small but significant effect on the equilibrium structure of the hydrogen-bonded water chain. During classical trajectories, proton transfer between consecutive water molecules is a very fast spontaneous process that takes place in the subpicosecond time scale. The translocation along extended regions of the chain takes place neither via a totally concerted mechanism in which the donor-acceptor pattern would flip over the entire chain in a single step, nor via a succession of incoherent hops between well-defined intermediates. Rather, proton transfer in the wire is a semicollective process that results from the subtle interplay of rapid hydrogen-bond length fluctuations along the water chain. These rapid structural fluctuations of the protonated single file of waters around an average position and the slow movements of the average position of the excess proton along the channel axis occur on two very different time scales. Ultimately, it is the slow reorganization of hydrogen bonds between single-file water molecules and channel backbone carbonyl groups that, by affecting the connectivity and the dynamics of the single-file water chain, also limits the translocation of the proton across the pore.

INTRODUCTION

Unique properties are displayed by proton translocation phenomena across biological membranes, implying that the mechanism underlying the conduction of protons is radically different from that of other ions (Levitt, 1984). Transport through the simple transmembrane channel formed by the gramicidin A molecule (GA) offers a particularly striking example of this phenomenon (Hladky and Haydon, 1972). The measured channel conductance to H^+ (530 pmho; see Akeson and Deamer, 1991) is more than 15 times that to potassium (29 pmho). [The maximum conductance to K^+ is approximately 29 pmho, based on previous experimental results (Hladky and Haydon, 1972; Finkelstein and Andersen, 1981; see also Roux and Karplus, 1991).] As shown in Table 1, such a difference is much larger than would be expected simply from the ratio of the mobility of these ions in bulk water. This is all the more remarkable, because the size of K^+ is similar to that of a hydronium ion OH_3^+. In fact, diffusion constants inside the pore deduced from experimental data suggest that protons move almost eight times as fast as water molecules themselves (see Table 1). Because of the narrowness of the pore, permeating waters or ions cannot pass each other inside the GA channel, and they must move in single file (Finkelstein and Andersen, 1981). The transport of a cation such as potassium is limited by the displacement of the single file of water molecules inside the channel; as shown in Table 1, the estimated diffusion constants of potassium ion or a water molecule inside the channel are nearly equivalent. In contrast, translocation of a proton does not in principle require the displacement of the single file of water molecules. Instead, the rapid translocation of protons across the GA channel is thought to occur through a succession of hops along the single file of hydrogen-bonded water molecules, which acts effectively as a proton wire (Hille, 1992).

The concept of proton wires was first introduced by Nagle and Morowitz to account for the fast conductance of protons along chains of hydrogen-bonded protonable groups in biological systems (Nagle and Morowitz, 1978) and includes the single file of water molecules that fill the narrow channels of transmembrane pores such as the GA channel (Akeson and Deamer, 1991). However, the biological relevance of water proton wires extends beyond the

Received for publication 5 December 1995 and in final form 14 March 1996.

Address reprint requests to Dr. Benoit Roux, Chemistry Department, Université de Montréal, C.P. 6128, succ. A, Montréal, Québec H3C 3J7 Canada. Tel.: 514-343-7105; Fax: 514-343-7586; E-mail: rouxb@ere.umontreal.ca.

0006-3495/96/07/19/21 $2.00

TABLE 1 Experimental diffusion constants

Species	Diffusion constants (Å²/ps)	
	GA channel*	Bulk water#
H_2O	4.4×10^{-3}	2.1×10^{-1}
K^+	1.9×10^{-3}	2.0×10^{-1}
H^+	3.4×10^{-2}	9.3×10^{-1}

*The water diffusion constant inside the GA channel was extracted from the experimental diffusional water permeability $P_w = 1.82 \times 10^{-15}$ cm³/s (Finkelstein and Andersen, 1981), using $P_w = DS/L$, with $L = 23$ Å and $S = 7.84$ Å². The cation diffusion constant inside the GA channel was extracted from the experimental maximum conductance using $\Lambda_{max} = De^2/k_BTL^2$, with $L = 23$ Å (see Roux and Karplus, 1991).
#From Hille (1992).

realm of transmembrane pores. The mediation of H^+ transfer by chains of water molecules is emerging in a wide range of proton transport phenomena involved in bioenergetics. It has been proposed that chains of water molecules could play important roles in the protonation of the Schiff base of the bacteriorhodopsin of *Halobacterium halobium* (Cao et al., 1991) and of the secondary quinone in the photosynthetic reaction center from *Rhodobacter sphaeroides* (Baciou and Michel, manuscript submitted for publication), and for the proton entry pathway into the cytochrome *b6f* complex of the plant chloroplast thylakoid membrane (Martinez et al., 1995). Moreover, the insight gained from the study of water wires may provide a better understanding of proton transfer processes in enzymes and in liquids in general.

Although kinetic models for hydrogen-bonded chains were proposed in the late 1970s (Nagle and Morowitz, 1978; Knapp et al., 1980), little is known at the present time about the detailed molecular mechanism of H^+ translocation along proton wires. Scheme 1 summarizes the problem at hand: (I) an excess proton is incorporated at one end of a single file of water molecules, and (II) a series of proton transfers takes place between adjacent water molecules until (III) a proton is released at the other end. Several questions

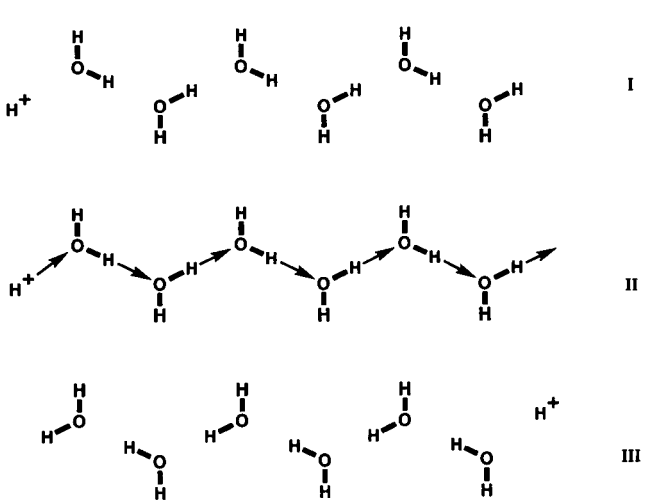

Scheme 1

come to mind. How does this translocation take place? What are the factors governing the translocation? What are the various steps and intermediates involved?

In the present work, we propose to study the properties of the proton wire of the channel formed by the GA molecules using computer simulations. The gramicidin A molecule is a synthetic polypeptide chain of 15 residues that associates as a dimer to form a pore spanning phospholipid bilayers (Urry, 1971), which has been extensively studied both experimentally and theoretically. The three-dimensional structure of the GA channel's ion-conducting state has been determined to atomic resolution by NMR spectroscopy (Arseniev et al., 1985; Ketchem et al., 1993). Over the past 15 years, the structural simplicity of the GA channel has stimulated the development of numerous theoretical studies (see the review by Roux and Karplus, 1994, and references therein), which have provided considerable insight into the mechanism of ion permeation. Problems ranging from the properties of the single-file solution filling the pore to the calculation of the rate of transport of ions have been addressed in ever-growing detail. In particular, several computational studies of the GA channel have stressed the important structural and dynamical properties of the linear chain of water molecules (MacKay et al., 1984; MacKay and Wilson, 1986; Kim, 1985; Etchebest and Pullman, 1986a, b; Pullman, 1987; Skerra and Brickman, 1987; Chiu et al., 1989, 1991, 1993; Jordan, 1990; Roux and Karplus, 1991, 1994; Roux, 1995).

In contrast with the insight gained from these studies, the detailed mechanism of H^+ translocation through the GA channel has remained an outstanding problem that has not been addressed at the molecular level. This is due to a combination of factors. To begin with, the treatment of proton transfer in water is a challenging theoretical problem, owing to the difficulty of accurately modeling the potential energy surface governing the dynamics and the dissociation of water aggregates. Traditional potential functions with harmonic bonds, such as the TIP3P and SPC models (Jorgensen et al., 1983; Berendsen et al., 1981), cannot account for these effects. High levels of ab initio calculation have revealed the complexity of the potential energy surface for the motion of protonated clusters of water molecules (Scheiner, 1985, 1994; DelBene, 1988; Komatsuzaki and Ohmine, 1994). In addition, this difficulty is compounded by the necessity of accounting for the quantum nature of the proton nuclei. To this effect, a number of ab initio quantum-classical methods have been proposed, which are very promising for the study of proton transfer in biological systems (see, for example, Bala et al., 1994; Mavri and Berendsen, 1995). However, these approaches are still too expensive for the study of proton translocation over the relatively long distances covered by biological proton wires. The use of discretized Feynman path integrals in conjunction with an empirical potential energy function makes it possible to overcome such a limitation. The path integral treatment allows the inclusion of the quantum effects arising from the light mass of protons and has been used by other

authors in studies of proton transfer along model hydrogen bonds (Lobaugh and Voth, 1992; Laria et al., 1994), as well as in an all-quantum study of small protonated water clusters published recently (Cheng et al., 1995). Moreover, previous studies have shown that the discretized Feynman path integral methodology can be used effectively in simulations of large protein systems, particularly to improve the treatment of hydrogen bonds (Zheng et al., 1989).

In two earlier papers, we described computer simulations of proton translocations along a linear chain of water molecules (Pomès and Roux, 1995, 1996). Discretized Feynman path integral molecular dynamics simulations (Feynman and Hibbs, 1965; Chandler and Wolynes, 1980) were used to account for the quantum nature of all the hydrogen nuclei of a linear protonated chain of hydrogen-bonded water molecules in vacuo. The polarization model, version 6 (PM6), developed by Stillinger and co-workers to reproduce the structure and dynamics of small water clusters (Weber and Stillinger, 1982), was employed to account for the polarization and dissociation of water molecules. The studies clarified the relative importance of quantum dispersion of the protons and of the flexibility of protonated water chains in vacuo.

In the present paper, we extend that model to study the single file of water molecules of the gramicidin A channel and its ability to function as a proton wire. The methodology used to represent the quantum dispersion of the proton nuclei and to generate molecular dynamics trajectories of the water-filled GA channel is reviewed in the next section. In the subsequent sections, the structure and dynamics of the single-file water chain with an excess proton are characterized. The importance of quantum effects, the interplay of local and cooperative fluctuations of the wire, and the influence of the channel environment are examined. The possibility of describing the proton translocation in terms of reaction coordinates is analyzed. This study concludes with the dynamics of proton translocation, and implications are considered for the molecular mechanism of H^+ conduction by the proton wires of GA and other water-filled biological channels. Efforts are made to relate the present study to previous theoretical models describing proton conduction in biological systems (Nagle and Morowitz, 1978; Knapp et al., 1980; Akeson and Deamer, 1991).

METHODOLOGY

Microscopic system

The simulation system includes the GA channel together with 22 water molecules and an excess proton. In all of the simulations reported here, the initial (reference) configuration was taken from a previous molecular dynamics simulation of the channel embedded in a dimyristoyl phosphatidylcholine (DMPC) bilayer (Woolf and Roux, 1994). The coordinates of the channel were initially derived from the Arseniev structure (Arseniev et al., 1985). The monomers assemble in head-to-head fashion to form a right-handed β-helix 20 Å in length with an inside diameter of 4 Å. The pore is lined with backbone peptide groups that form 20 intramonomer and six intermolecular hydrogen bonds. The 22 water molecules within 15 Å of the center of the channel from the GA:DMPC configuration were kept. Of these, 10 were located in the single-file region and six were in each mouth.

The overall translation of the molecular system was avoided by forcing the center of mass of the dimer to coincide with the origin by means of a strong harmonic constraint. Moreover, the center of mass of each monomeric unit was similarly restrained to remain along the z axis so as to ensure the alignment of the channel with that axis and suppress two rotational degrees of freedom of the channel. Finally, weak harmonic constraints of 0.1 kcal/mol/Å^2 were also imposed on each heavy atom of the tryptophan side chains so as to confine them to the vicinity of their position in the initial, reference structure. These weak energy restraints were required to ensure that the channel would retain its β-helical dimer conformation in the absence of an explicit membrane environment. In a long preliminary simulation performed without this restraint, the tryptophan side chains were observed to travel and distort the channel's mouths, resulting in the unfolding of the channel after several tens of picoseconds, which is inconsistent with simulations performed in an explicit membrane environment (Woolf and Roux, 1994, 1996).

In the reference configuration, 10 water molecules were located inside the channel in single-file fashion, whereas 6 water molecules made up small solvent caps at either end of the channel. These caps were restrained to lie in the region of the mouths of the gramicidin channel by cylindrical constraints: all of the water oxygen atoms were subjected to soft quadratic restoring potentials beyond 5 Å from the channel axis, and beyond planes perpendicular to the channel axis at $z = \pm 15$ Å from the origin at the center of the pore. These restraints prevented the evaporation of cap waters or their incursion into regions normally occupied by the hydrocarbon chains around the channel, without affecting the single-file water molecules.

Potential energy function

The total interaction energy is given by $U_{\text{total}} = U_{\text{water}} + U_{\text{channel}}$. The force field of the CHARMM program (Brooks et al., 1983), version 22, was employed for the protein (U_{channel}). The potential energy surface U_{water} governing the motion of the water oxygen and hydrogen nuclei was modeled with the polarization model (PM6) of Stillinger and co-workers (Stillinger and David, 1978; Stillinger, 1979; Weber and Stillinger, 1982). This model was initially developed and parameterized to accurately reproduce the structure and energy of small hydrogen-bonded cationic and anionic water clusters. The basic structural elements of PM6 are H^+ and O^{2-} atoms, which makes it possible to account for the full dissociation of water molecules into ionic frag-

ments. For a configuration of the oxygen and hydrogen constituents with coordinates $\{\mathbf{r}_O\} \equiv \{\mathbf{r}_{O_1}, \ldots, \mathbf{r}_{O_{NO}}\}$ and $\{\mathbf{r}_H\} \equiv \{\mathbf{r}_{H_1}, \ldots, \mathbf{r}_{H_{NH}}\}$, and a channel configuration given by $\{\mathbf{r}_X\} \equiv \{\mathbf{r}_{X_1}, \ldots, \mathbf{r}_{X_{NX}}\}$, the PM6 potential energy is

$$
\begin{aligned}
&U_{\text{water}}(\{\mathbf{r}_O\}, \{\mathbf{r}_H\}, \{\mathbf{r}_X\}) \\
&= \sum_{i<j=1}^{N_O} \phi_{OO}(|\mathbf{r}_{O_i} - \mathbf{r}_{O_j}|) + \sum_{i<j=1}^{N_H} \phi_{HH}(|\mathbf{r}_{H_i} - \mathbf{r}_{H_j}|) \qquad (1)\\
&+ \sum_{i=1}^{N_O}\sum_{j=1}^{N_H} \phi_{OH}(|\mathbf{r}_{O_i} - \mathbf{r}_{H_j}|) + \sum_{i=1}^{N_O}\sum_{j=1}^{N_X} \phi_{OX}(|\mathbf{r}_{O_i} - \mathbf{r}_{X_j}|) \\
&+ \sum_{i=1}^{N_H}\sum_{i=1}^{N_X} \phi_{HX}(|\mathbf{r}_{H_i} - \mathbf{r}_{X_j}|) + \Phi_{\text{pol}}(\{\mathbf{r}_O\}, \{\mathbf{r}_H\}, \{\mathbf{r}_X\}),
\end{aligned}
$$

where ϕ_{OO}, ϕ_{OH}, and ϕ_{HH} are the PM6 pairwise radially symmetric functions (Weber and Stillinger, 1982), and ϕ_{OX} and ϕ_{HX} are pairwise radially symmetric functions constructed from PM6 and the CHARMM force field. ϕ_{OX} and ϕ_{HX} correspond to the nonbonded Lennard-Jones and direct Coulomb interactions between the channel atoms and the water nucleus (see below).

Φ_{pol} represents a many-body polarization energy contribution resulting from the polarization of the water oxygen particles,

$$
\Phi_{\text{pol}}(\{\mathbf{r}_O\}, \{\mathbf{r}_H\}, \{\mathbf{r}_X\}) = -\frac{1}{2}\sum_{i=1}^{N_O} \mu_{O_i} \cdot \mathbf{G}_i^{(L)}, \qquad (2)
$$

where

$$
\mathbf{G}_i^{(L)} = \sum_{\substack{j=1 \\ j\neq i}}^{N} \frac{q_j \mathbf{r}_{ij}}{r_{ij}^3}[1 - L(r_{ij})] \qquad (3)
$$

is an effective field arising from surrounding particles. In this equation, $N = N_O + N_H + N_X$ is the total number of particles in the system, $\vec{r}_{ij} = \vec{r}_i - \vec{r}_j$ and $r_{ij} = |\mathbf{r}_{ij}|$ is the distance between atoms i and j, and $L(r)$ is a parametric damping function that accounts for the spatial extension of the electronic cloud surrounding each water oxygen atom (Stillinger, 1979). The induced atomic dipole moments, μ_{O_i}, are determined self-consistently from the following set of equations for the oxygen atoms O_i:

$$
\mu_{O_i} = \alpha \mathbf{G}_i^{(K)}, \qquad (4)
$$

where

$$
\mathbf{G}_i^{(K)} = \sum_{\substack{j=1 \\ j\neq i}}^{N} \frac{q_j \mathbf{r}_{ij}}{r_{ij}^3}[1 - K(r_{ij})] + \sum_{\substack{k=1 \\ k\neq i}}^{N_O} \frac{T_{ik}\mu_k}{r_{ik}^3}[1 - K(r_{ij})]. \qquad (5)
$$

Here, α is the polarizability of water oxygen atoms, $K(r)$ is a parametric damping function similar to $L(r)$, and T_{ik} is the dipole-dipole tensor term for each O_i-O_k pair (Stillinger, 1979). It should be noted that the potential energy governing the motion of the water oxygen and hydrogen, including the water-channel coupling, involves many-body interactions due to Eqs. 2–4.

The combination of the water (polarizable-dissociable) and channel (molecular mechanical) potentials is similar to that described in hybrid quantum-mechanical/molecular mechanical (QM/MM) approaches, in which an semiempirical quantum mechanical potential is coupled to a molecular mechanical force field (Field et al., 1990; Gao and Xia, 1992). An underlying assumption in the present model is that proton exchange reactions from the channel to the water do not play a dominant role in the transport mechanism. Indeed, dissociation and association events involving the amide and the carbonyl groups of the channel backbone cannot occur, because of the choice of the molecular mechanical potential function, and are ignored. This approximation is supported by nuclear magnetic resonance studies which indicate that the intrinsic rate of exchange of amide protons that are freely accessible to the solvent is estimated to vary between 1 and 10 min^{-1} (Wüthrich, 1986), or between 10^{-1} and 10^{-3} s^{-1} (Jeng and Englander, 1991) in the pH range 1–6. This is considerably slower than the estimated rate for proton diffusion in the channel (Table 1). Therefore, it seems unlikely that proton exchange with the channel backbone could play a determining role in the function of the GA proton wire.

The relative strength of water-water, channel-water, and channel-channel interactions, in particular where hydrogen bonds are concerned, has been shown to be critical to the properties of the water single file of the gramicidin channel (MacKay et al., 1984). These properties are also affected by the incorporation of polarizability (Jordan, 1990). Lennard-Jones parameters governing the water-channel pairwise nonbonded interactions described by ϕ_{OX} and ϕ_{HX} were adjusted after the interaction of a single water molecule with *N*-methylacetamide (NMA) taken as a model of the channel backbone. Specifically, a fit of the effective Lennard-Jones radius σ governing the Lennard-Jones interaction between water oxygen and backbone hydrogen atoms was performed so as to approximately reproduce the geometric and energetic properties of the $NH \cdots OH_2$ hydrogen bond of the water-NMA dimer, whereas the Lennard-Jones radius for all other water-channel interactions was identical to that defined in the TIP3P (Jorgensen et al., 1983) and CHARMM (Brooks et al., 1983) models. The results for water-NMA hydrogen bonds are given in Table 2, where they are com-

TABLE 2 Water-NMA hydrogen bonds

	N-Methylacetamide			
	C = O		N-H	
Water model	d (Å)	E (kcal/mol)	d (Å)	E (kcal/mol)
Ab initio[a]	1.88	−7.3	1.99	−5.4
TIP3P	1.77	−7.2	1.93	−5.6
PM6	1.99	−8.6	1.94	−6.5

[a]Results of HF/6–31G* calculations from Guo and Karplus (1992).

pared to the optimized values obtained with ab initio calculations at the HF/6–31G* level (Guo and Karplus, 1992) and with the TIP3P model. The energy and distance of the water-carbonyl hydrogen bond represent a compromise with respect to results obtained from ab initio calculations. The PM6 result overestimates both the length (by 0.11 Å) and the absolute energy (by 1 kcal/mol). On the other hand, the optimized PM6 geometry of the $NH \cdots OH_2$ hydrogen bond is comparable to that of TIP3P, although the energy is overestimated, again by about 1 kcal/mol. A comparison of the results obtained with the present model and previously published results will be provided in the Discussion.

Discretized Feynman path integral

The importance of quantum effects was investigated by exploiting the isomorphism of the discretized Feynman path integral representation of the density matrix with an effective classical system obeying Boltzmann statistics (Feynman and Hibbs, 1965; Chandler and Wolynes, 1980). Molecular dynamics simulations of the effective classical system are valid for obtaining ensemble averages, although they do not provide information on the time-dependent quantum dynamics of the system. Only the quantization of the water hydrogen nuclei was considered, and the water oxygens, as well as all the atoms the channel (hydrogen atoms included), were treated as classical particles. Following the path integral approach, each proton was replaced in the effective classical system by a ring polymer, or necklace, of P fictitious particles with a harmonic spring between nearest neighbors along the ring. The potential energy of the effective classical system is

$$U_{\text{eff}}(\{\mathbf{r}_O\}, \{\mathbf{r}_H^{(1)}\}, \ldots, \{\mathbf{r}_H^{(P)}\}, \{\mathbf{r}_X\}) = U_{\text{channel}}(\{\mathbf{r}_X\}) + \frac{1}{P}\sum_{p=1}^{P} U_{\text{water}}(\{\mathbf{r}_O\}, \{\mathbf{r}_H^{(p)}\}, \{\mathbf{r}_X\}) + \sum_{i=1}^{N_H}\sum_{p=1}^{P}\frac{1}{2}K_{\text{polymer}}|\mathbf{r}_{H_i}^{(p)} - \mathbf{r}_{H_i}^{(p+1)}|^2, \quad (6)$$

where $\{\mathbf{r}_H^{(p)}\} = \mathbf{r}_{H_1}^{(p)}, \ldots, \mathbf{r}_{H_{N_H}}^{(p)}$ represents the coordinates of the pth particle for protons H_1 through H_{N_H}, and $K_{\text{polymer}} = PM_H(k_BT/\hbar)^2$ is the harmonic spring constant acting between the pth and $(p + 1)$th nearest neighbors along the polymer necklace representing each proton H_i of mass M_H. In the third summation of Eq. 6, $\mathbf{r}^{(P+1)} \equiv \mathbf{r}^{(1)}$ is required to satisfy the closure of the ring polymers. In the present path integral simulations, each water hydrogen nucleus was represented as a polymer necklace of $P = 32$ fictitious particles. This number contrasts with previous path integral simulations of water in which only three fictitious particles per hydrogen were used to study the quantization of the rotational and librational motions of rigid water models (Kuharski and Rossky, 1985). A much larger number is necessary in the present study, because high-frequency bond stretching modes are included. A discretization of the path integral with 20 to 30 fictitious particles was found to be adequate in recent path integral studies of proton transfer in model systems (Lobaugh and Voth, 1992; Azzouz and Borgis, 1992; Laria et al., 1994). The total number of particles in the simulation system was 618 and 619, respectively, in the unprotonated and protonated classical systems ($P = 1$) and 2014 in the quantum system ($P = 32$).

In the quantum simulations ($P = 32$), the configurational sampling was performed by generating Langevin molecular dynamics trajectories of the effective system. The choice of Langevin dynamics was dictated by the need to avoid the nonergodicity of path integral molecular dynamics simulations based on the microcanonical ensemble (Allen and Tildesley, 1987). For all degrees of freedom x_α in the effective classical system, the trajectory was calculated according to the Langevin equation of motion:

$$m_\alpha \ddot{x}_\alpha = -\partial x_\alpha U_{\text{eff}} - \gamma \dot{x}_\alpha + f(t), \quad (7)$$

where γ is a friction constant and $f(t)$ is a random Gaussian force obeying the fluctuation-dissipation theorem:

$$\langle f(t)f(0)\rangle = 2k_BT\gamma\delta(t). \quad (8)$$

This simulation ensures that the configurations were generated according to a Boltzman distribution, $\exp[-U_{\text{eff}}/k_BT]$, at temperature T. It should be noted that the resulting Boltzmann distribution is independent of the choice of dynamical mass m_α attributed to each degree of freedom. By contrast, in the simulations performed in the classical limit ($P = 1$), the equations of motion were propagated in the microcanonical ensemble. Deterministic trajectories offer the advantage, over stochastic ones, that dynamical information, not just thermodynamic averages, can be extracted from the computer simulation.

During the propagation of the trajectories of the effective system, the full PM6 potential function, $U_{\text{water}}(\{\mathbf{r}_O\}, \{\mathbf{r}_H^{(p)}\}, \{\mathbf{r}_X\})$, was recalculated for each p-step of the discretized path integral (Eq. 4). In particular, the interactions involving the pairwise interactions ϕ_{HH} and ϕ_{OH} were recalculated. It is important to note that the polarization energy contribution, $\Phi_{\text{pol}}(\{\mathbf{r}_O\}, \{\mathbf{r}_H^{(p)}\}, \{\mathbf{r}_X\})$, was determined by solving a set of self-consistent equations (Eq. 4) for each value of p. In other words, each molecular dynamics time step involved the determination of 32 polarization states induced on the set of 22 oxygen atoms. The forces on all particles due to the many-body polarization were calculated analytically by solving a similar set of self-consistent equations derived by Stillinger (1979). For the sake of computational efficiency, other contributions arising from constant terms, such as the PM6 oxygen-oxygen ϕ_{OO} and channel-water interactions, were calculated only once and stored.

Computational details

Molecular dynamics trajectories were generated using the integration schemes described above. The time step used for

the integration of the equations of motion was 0.0005 ps. This short time step is made necessary by the high frequency of O-H vibrations in PM6 waters. No SHAKE restriction was applied on chemical bond vibrations. Calculations were performed on a Silicon Graphics R4400 workstation. The propagation of the classical trajectories required about 15 min of cpu time per picosecond, and that of the quantum trajectory, about 6 h per picosecond. The temperature of the bath was 300K. Initial velocities were assigned at random from a Gaussian distribution. In the equilibration (early) phase of the simulations, the velocities were reassigned every 200 steps, whereas in the production phase the temperature simply fluctuated within 10K of the 300K mean in the classical (Verlet) simulations.

The equilibrations were performed as follows. First, PM6 water molecules were substituted for the original TIP3P (Jorgensen et al., 1983) water molecules used in the reference configuration (Woolf and Roux, 1994). The position of the water hydrogen nuclei were optimized by steepest-descent energy minimization performed with all other atoms fixed. The minimization procedure was repeated with all water atoms allowed to move, and the solvent was thermalized at 300K for 5 ps. The polypeptide channel atoms were then allowed to move, and the whole system was equilibrated for a period of 20 ps. From this configuration, four distinct trajectories were created. These trajectories are summarized in Table 3 and will be referred to henceforth as trajectories A, B, C, and D. The production stage of trajectory A was generated directly without an additional proton, whereas the other simulations included an excess hydrogen nucleus. In addition, trajectory C included a quantum treatment of all water hydrogen nuclei ($P = 32$), and trajectory D was propagated in the absence of the electrostatic field created by the partial charges $\{q_X\}$ of channel atoms X in the calculation of $\Phi_{pol}(\{\mathbf{r}_O\}, \{\mathbf{r}_H\}, \{\mathbf{r}_X\})$ and of the direct nonbonded coulomb interaction in ϕ_{OX} and ϕ_{HX} (Eqs. 1–5). The water-channel nonbonded Lennard-Jones interactions were kept unchanged. This artificial model maintains the GA structure but removes the electrostatic interactions giving rise to water-channel hydrogen bonding. For this reason, the simulation D can be thought of as a proton wire in the interior of a "hydrophobic channel" that is both structurally and dynamically equivalent to the GA channel.

To construct trajectories B, C, and D, an excess proton was inserted into the single file of water molecules. A site was selected in the middle of a monomer between water oxygen atoms O7 and O8, at $z = 5.29$ Å. Two energy minimization cycles were then imposed, first with only the hydrogen nuclei being allowed to move, and again with rigid constraints on the channel only. The two-stage equilibration process was then repeated, once for the water and again for the whole system. The equilibration of system C was performed after superposition of 31 extra p-particles to each of the classical water hydrogen nuclei. The production stages followed, for up to 400 ps for the classical simulation B, and 100 ps for the quantum simulation C. The fourth trajectory (D) was performed to examine the importance of water-channel interactions on the translocation mechanism. From the equilibrated configuration obtained with simulation B, the nonbonded channel-water coulomb interactions and the channel-water components of the polarization function were turned off, and a 200-ps trajectory was produced after an additional two-stage equilibration.

TABLE 3 Description of the computer simulations

Code	P	Excess proton?	U_{elec} off?	Total time (ps)
A	1	No	No	200
B	1	Yes	No	400
C	32	Yes	No	100
D	1	Yes	Yes	200

RESULTS AND DISCUSSION

Structure of the gramicidin channel

The channel retained its β-helix structure over the hundreds of picoseconds spanned by each of the four molecular dynamics trajectories. Moreover, the average (ϕ, ψ) values of the C_α angles were very similar for trajectories A, B, and C, indicating that the integrity of the channel is altered neither by the inclusion of an excess proton, nor by a quantum treatment of water hydrogen nuclei. On the other hand, the structure of the channel was slightly affected by the disappearance of electrostatic interactions with the linear water chain. Minor differences in the channel conformation (10° to 15°) arose in trajectory D, where no hydrogen bonds could be formed between the channel and water molecules. A statistically representative configuration of the trajectory C is shown in Fig. 1.

In all of the simulations, the near-symmetry of the channel with respect to its center at the dimer junction was evident in both the average conformation and backbone fluctuations. The average rms fluctuations of the ϕ and ψ torsions were of about 8° or 9° near the center of each pentadecapeptide monomer. The channel mouths, and above all the region of the dimer junction (residues 1 to 5 of each gramicidin monomer), were significantly more mobile, with backbone torsions fluctuating up to twice as much. A good agreement was observed among the various trajectories, although the absence of water-channel hydrogen bonds in simulation D resulted in somewhat more uniform fluctuations of 10° to 12° throughout the channel. This analysis suggests that the fine structure of water-channel interactions can modulate the local flexibility of the backbone, not only at the mouths of the pore but also in the single-file region. In turn, the librational motion of the backbone CO groups has been shown to have a strong influence on the dynamics of the single file (Chiu et al., 1991).

The lipid bilayer has a profound influence on the stability and the dynamics of the channel. To date, only one computational study of the GA channel included the lipid matrix, together with a large number of water molecules and periodic boundary conditions (Woolf and Roux, 1994,

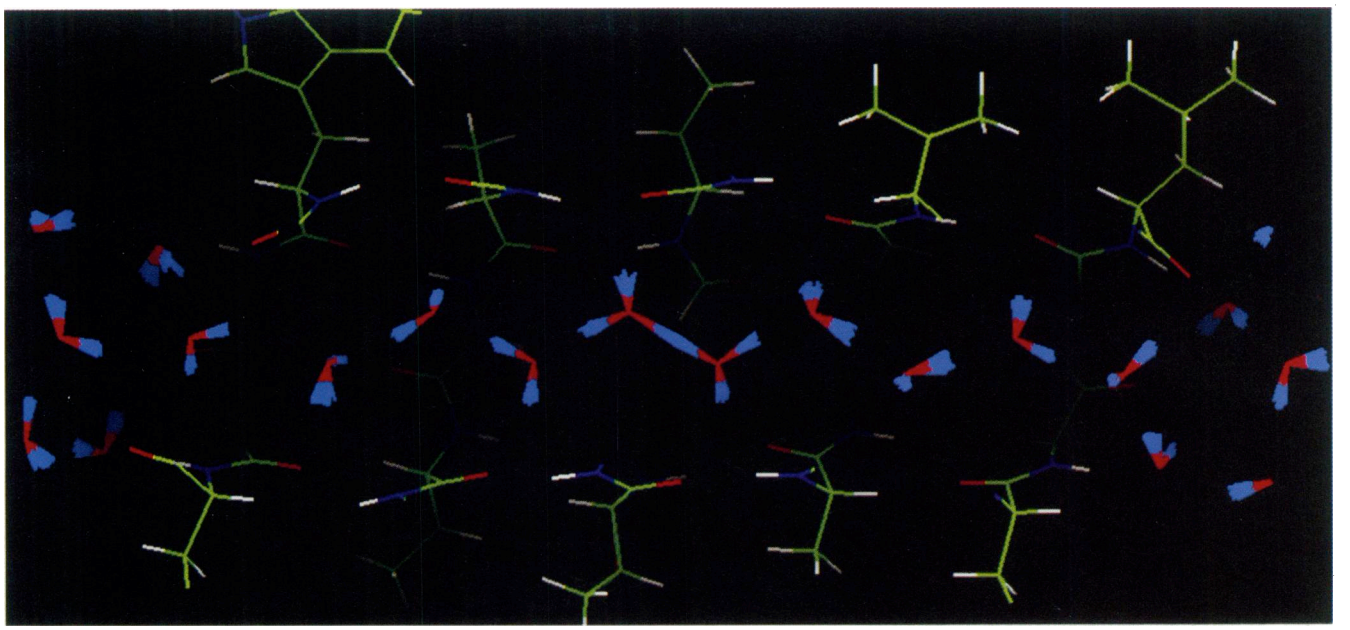

FIGURE 1 Cross section of the gramicidin A channel with 22 water molecules and an excess proton. The axis of the channel, z, runs from left to right. This snapshot was taken from a quantum Feynman path integral molecular dynamics simulation, in which the water hydrogen nuclei are modeled by flexible ring polymers (light blue). In this configuration, H^+ is solvated by two water molecules in a $O_2H_5^+$ ion located near the center of the channel.

1996). The starting configuration for the present study was chosen from the equilibrated part of that trajectory and reflects the influence of the lipid bilayer. It is not possible to preserve the long-term integrity of the channel structure during a simulation in vacuo without incorporating the influence of the membrane, if only approximately. To compensate for the omission of the membrane, weak harmonic constraints were imposed on the position of the tryptophan side-chain atoms, so as to preserve the long-term integrity of the channel. Although in principle our positional restraints on Trp side chains necessarily limit the extent of backbone torsional freedom, they do not by any means prevent the fluctuations of channel backbone groups, or the rearrangement of channel-water hydrogen bonds, as we will see in the analysis of the trajectories.

Structure of the single file

Statistically representative configurations of the water molecules are shown in Figs. 1 and 2, and the average atomic distributions of water O and H particles along the channel axis are shown in Fig. 3. The distributions of single-file water oxygen atoms obtained from trajectories A through C are very similar. There are on average 10 water molecules in the single-file region in all three simulations A, B, and C (Fig. 2). In addition, two water molecules mark the ends of the channel at $z \simeq \pm 12$ Å; these two water molecules are off the axis of the channel and provide an interface with the mouth region rather than forming part of the single file per se. Five water molecules complete the solvent "caps" at each end of the channel.

In the unprotonated case A, Fig. 2 shows that there is a continuous and monodirectional donor-acceptor pattern of hydrogen bonds linking single-file water molecules 1 through 9. This pattern breaks down at molecule 9, which does not form a good hydrogen bond with water 10. These observations hold over the entire trajectory A, as the structure displayed in the average density of oxygen and hydrogen particles shows (Fig. 3 *A*). Moreover, the discrete nature of the water oxygen density in the single-file region indicates that there is no significant diffusion of waters during the simulation. Rather, the regular shape and spacing of the oxygen peaks suggest that each oxygen atom fluctuates around a well-defined mean position on the z axis. We note two exceptions to the regularity of oxygen density peaks: water number 9 is less mobile (sharper distribution of the oxygen peak), whereas water molecules 1 and 2 are more mobile, with possibly two nearly spaced favored locations along the z axis for each of them. The asymmetry of the distributions reflects the lack of convergence due to the finite length of the simulations.

The quasiperiodic distribution of the single-file water oxygen atoms arises from both water-water and water-channel interactions. Hydrogen bonding between adjacent water molecules is marked by the relative positions of O and H peaks in the single-file region. The regular donor-acceptor pattern linking waters 1 through 9 noted above is evidenced by the alternance of the peaks. Additionally, OH bonds not involved in the water-water hydrogen-bonded chain are oriented roughly perpendicularly to the channel axis (resulting in overlapping O and H densities in Fig. 3) and engage in hydrogen bonds with the channel backbone

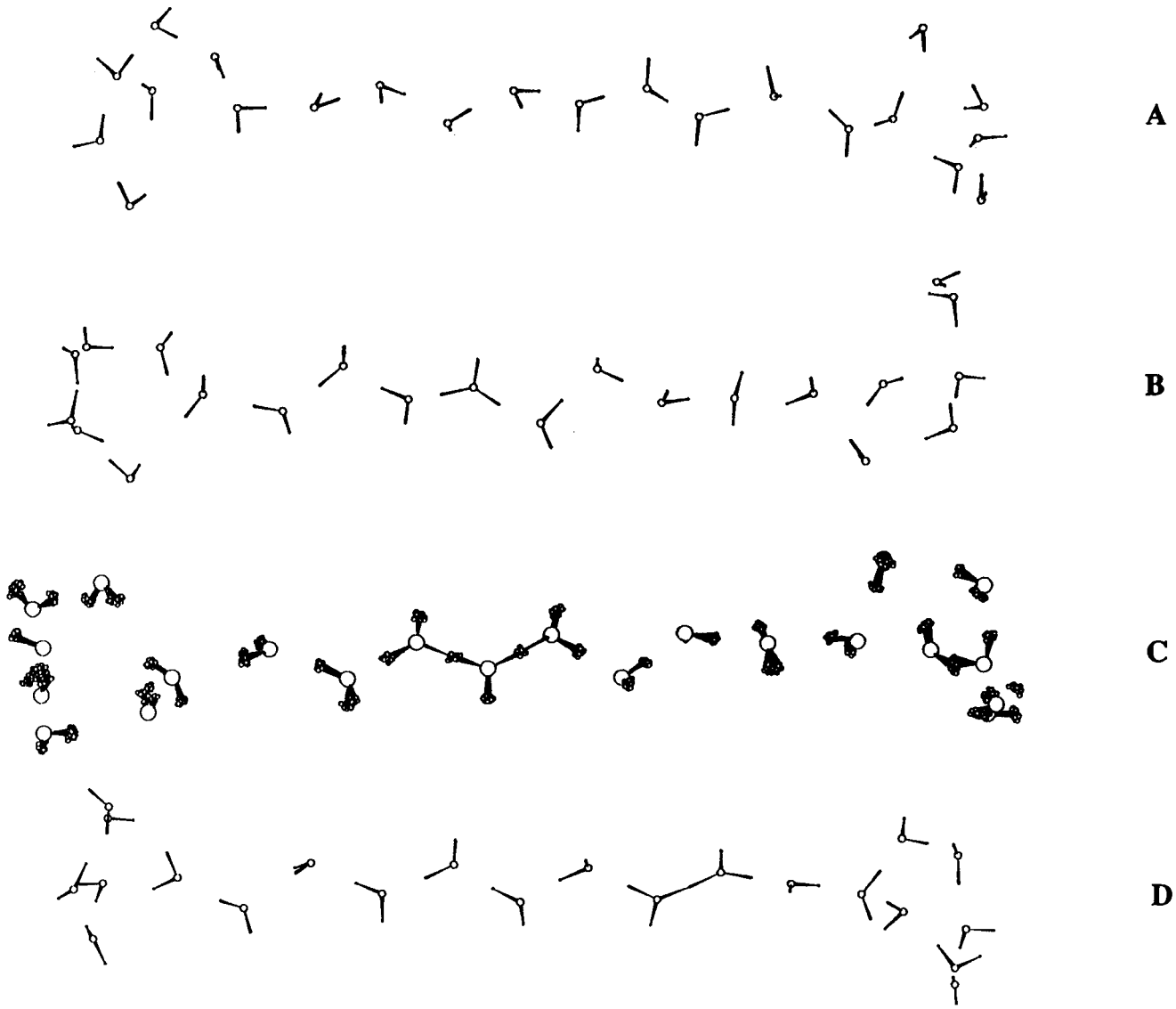

FIGURE 2 Snapshots of water configurations obtained, respectively, from simulations A, B, C, and D. The single-file region of the pore contains a hydrogen-bonded chain of 10 water molecules. In configurations B, C, and D, the excess proton is solvated in OH_3^+, $O_3H_7^+$, and $O_2H_5^+$ ions, respectively. Note how the donor-acceptor pattern of hydrogen bonds inverts around these ions.

oxygen atoms lining the interior of the pore. The helicity of the backbone is recovered in the spacing of oxygen density peaks along the channel axis. A 4.5-Å spacing along the axis corresponds to six residues in the channel backbone, approximately one turn in the helix, and two single-file water molecules.

It is desirable to compare the results obtained here on the unprotonated system A to previous computational studies of the gramicidin channel. These studies have been reviewed recently (Roux and Karplus, 1994), so that here we only emphasize the results pertinent to the properties of the proton wire. Previous studies concluded that eight to ten water molecules are present in the single-file region of the GA channel, in accordance with experimental results and with the present study. Numerous hydrogen bonds were observed between backbone carbonyl oxygen atoms and water molecules. Furthermore, the single-file water molecules were found to be oriented the same way (i.e., in a consistent donor-acceptor pattern) in most studies. However, gaps and defects in the hydrogen-bonded chain were observed, very consistently in the most realistic study (Roux and Karplus, 1994) and in another study including polarization of the water molecules (Jordan, 1990), and more infrequently with two other models (Chiu et al., 1989; Fornili et al., 1984). The restriction imposed to prevent the evaporation of the small water caps also prevents the possibility of net water diffusion over the course of the simulations. Although this would constitute a serious limitation in an investigation of long-term transport properties, previous studies indicate that the structure of the single file can be reasonably well characterized over the few hundreds of picoseconds spanned by each trajectory. Because the exper-

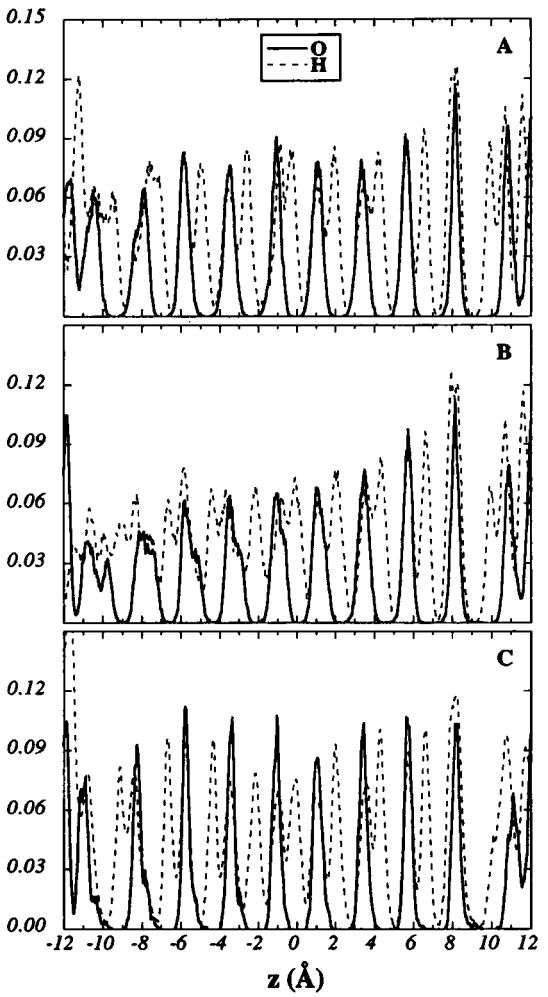

FIGURE 3 Distribution of water oxygen (bold) and hydrogen (dashed) particles along the channel axis obtained, respectively, from simulations A, B, and C. In all three cases, the 10 single-file water molecules are located between $z = -11.5$ and $z = 11.5$. Hydrogen bonding between water molecules is characterized by alternating O and H peaks, whereas water-channel hydrogen bonds correspond to nearly overlapping O and H densities. In cases B and C, the presence of an excess proton induces strong hydrogen bonds in which the proton is located halfway between two oxygen atom, notably at $z = -2$.

imentally determined mobility of water molecules (see Table 1) corresponds to water displacements of about 2 Å over 100 ps, much longer trajectories would be required to observe net diffusion.

Influence of an excess proton

In the following analysis we examine the effect of adding of a proton to the single file. In all three simulations B, C, and D, the presence of an excess H^+ affects hydrogen bonding among the single-file water molecules. In the particular configuration of Fig. 2 *B*, the protonated species appears to be a hydronium ion H_3O^+, around which the donor-acceptor pattern of the chain inverts, with OH bonds pointing away from the ion. The fine structure of the protonated chain will be discussed below, but we note here that in spite of the differences in charge and hydrogen-bonded structure of the single-file water chain, the average distribution of water O atoms along the z axis is remarkably similar in simulations A and B (compare Fig. 3, *A* and *B*). The somewhat broader shape of the peaks in Fig. 3 *B* arises in part from a longer time of simulation with respect to simulation A (400 ps versus 200 ps), and the mean position of most oxygen atoms is nearly identical in the two simulations. There is, however, significantly more mobility of oxygen atoms O1 through O5, with two distinct peaks for O1, corresponding to alternate hydrogen bonding with water 2 (right peak) and with the mouth water at $z \simeq -12$ Å (left peak). In the single file of B, there are thus two defects in the linear hydrogen-bonded chain, one between waters 9 and 10, and the other alternatively between 1 and 2 and between 1 and the water at the channel mouth.

The analysis of single-file hydrogen atom distributions in Fig. 3 *B* provides further information on the influence of an excess proton. Again, the hydrogen bond donor-acceptor organization is reflected in the relative locations of O and H peaks. Remarkably, the hydrogen distribution between waters 4 and 5 is located halfway between the oxygen peaks, indicating that sampling might be dominated by cases in which the proton is shared by two water molecules in a $O_2H_5^+$ cluster. On either side of that cluster, the hydrogen bonding pattern inverts, as noted earlier from Fig. 2 *B*.

In the isomorphic path integral treatment of simulation C, the hydrogen nuclei are represented by flexible ring polymers or necklaces of beads or *p*-particles. The average distribution of the *p*-particles corresponds to the quantum dispersion of the hydrogen nuclei. From the snapshots shown in Figs. 1 and 2 *C*, it is observed that the spatial dispersion of hydrogen nuclei in the water chain ranges from 0.2 to 0.5 Å. These conformations suggest tight solvation of the excess proton by two water molecules in $O_2H_5^+$, or in the less likely arrangement of a linear $O_3H_7^+$ cluster, in which two hydrogen nuclei are shared by three oxygen atoms.

The defect in the linear hydrogen-bonded chain observed in the previous cases subsists, with the orientation of the plane of molecule 9 perpendicular to the axis of the channel. As before, hydrogen-bonding features within the proton wire are visible in the density of single-file atoms (Fig. 3 *C*). The oxygen peaks are sharper than in Fig. 3 *B* because of the shorter simulation time (100 ps versus 400 ps), but they are located at the same positions along the z axis as in cases A and B. Delocalization in the position of hydrogen nuclei halfway between two oxygen peaks is evident for the O4–O5 hydrogen bond, and to a lesser extent for O5–O6. This suggests that the presence of an excess proton together with quantum treatment favors the emergence of tight $O_2H_5^+$, and perhaps $O_3H_7^+$, clusters inside the channel.

Finally, in the artificial "hydrophobic channel" simulation D, where the electrostatic interactions between the channel and water molecules were turned off, the absence of hydrogen bonds between the single-file water molecules

and the channel backbone results in a better connectivity of the hydrogen-bonded water chain. In the configuration shown in Fig. 2 *D*, the protonated water cluster resembles an $O_2H_5^+$ ion, with the excess proton located halfway between two water molecules, in a strong hydrogen bond. Unlike the results obtained from the other simulations, there are no interruptions in the hydrogen-bonded chain across the single-file region. In addition, the absence of water-channel hydrogen bond results in the greater translational freedom of individual water molecules, whose density along the channel axis (not shown) displays practically no structure compared to those obtained from trajectories A through C. The importance of water-channel hydrogen bonds is examined in more detail below.

Channel-water hydrogen bonds

Hydrogen bonding among water molecules and between channel polar groups and water molecules is illustrated in Fig. 4. This configuration was obtained from trajectory C. Each of the two water molecules forming a protonated dimer forms hydrogen bonds with its water neighbors in the single file, and one with a backbone carbonyl atom. Similar interactions are also shown for the adjoining water molecules. Although water-channel hydrogen bonds limit the location of water molecules along the channel axis over the time of the simulation, they do not preclude local deformations in the proton wire, as the irregularity of water-water hydrogen-bonding distances shows.

A systematic characterization of channel-water and water-water interactions can be gained through the study of atom-atom radial distribution functions. Because the water is in single file, no radial normalization was used; the *i-j* atom-atom function simply measures the relative probability of finding any atom of type *j* at a distance r_{ij} from any atom *i*, averaged over the number of type *i* atoms and over the total number of configurations. The atom-atom distributions of the distances between channel backbone carbonyl oxygen atoms and single-file water oxygen and hydrogen particles obtained from simulations A through C are shown in Fig. 5. The hydrogen bonds formed between the channel and the single-file water molecules are notably consistent in all three cases. All three O-O distributions have the same structure and peak sharply at 2.95 Å. The presence of an excess proton results in a better-defined O-O peak in cases B and C, compared to case A. The structure of O-H distributions is similar; the first peak at 1.9 to 2.0 Å matches the O-O peak in area, and together they define well-aligned

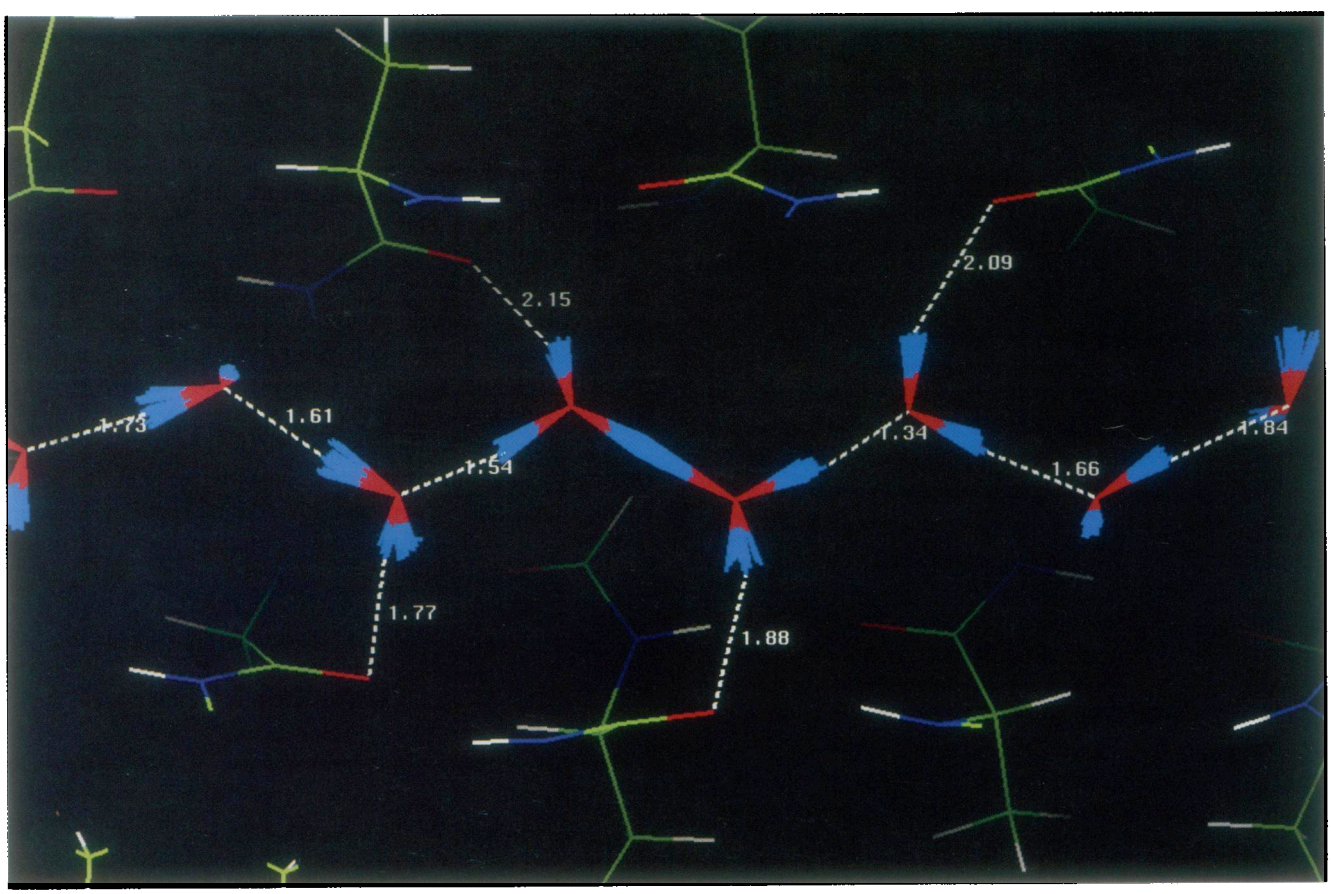

FIGURE 4 Hydrogen bonds involving single-file water molecules in the GA channel. This configuration is identical to the one shown in Fig. 1. The average dispersion of the Feynman path integral polymers (light blue) is about 0.3 Å. In general, each water molecule forms two hydrogen bonds with its neighbors in the single file, and one with a carbonyl oxygen atom on the backbone.

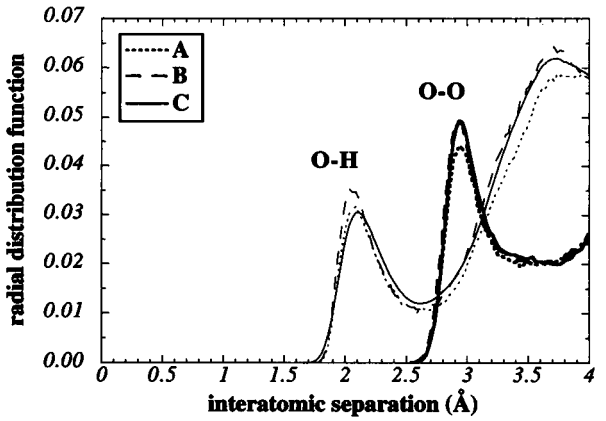

FIGURE 5 Atom-atom radial distribution functions between carbonyl oxygen atoms and water oxygen atoms (bold), and between carbonyl oxygen atoms and hydrogen nuclei (thin), obtained from simulations A, B, and C.

O-HO hydrogen bonds. The net charge of the excess H^+ results in a sharper O-H peak for B compared to A, whereas in case C this effect is overcompensated by quantum dispersion of hydrogen atoms, and the O-H peaks are notably broader. In case D (not shown) there is no hydrogen-bonding structure because, by design, the water-channel electrostatic interactions were turned off.

Water-water hydrogen bonds

The average O-O and O-H radial distributions between single-file water particles are shown in Fig. 6. In case A, the O-O distribution peaks at 2.75 Å, and the tail indicates that in some cases the O-O separation was as long as 3.4 Å (defect in the hydrogen-bonded chain). The first two peaks in the O-H distribution are well defined and correspond, respectively, to covalent bonding at 1.0 Å and hydrogen bonding with a H-donor at 1.6 Å.

A striking difference appears when an excess H^+ is present in the wire. The hydrogen-bonding structure described for A is also observed in case B, but in the latter case there are two new peaks, which correspond to a short hydrogen bond with an O-O separation of about 2.50 Å and an O-H separation of 1.2–1.3 Å. Thus the O-H peak is located at separations intermediate between those of covalent and hydrogen-bonding densities, halfway between two oxygen atoms. Note that this new O-H peak connects the covalent and hydrogen-bonding distributions, which indicates that during simulation B, effective proton translocations took place. Integration of these "short hydrogen bond" O-H and O-O peaks in the distribution function indicates that there is only one proton engaged in transfer on average, out of the seven or eight hydrogen atoms involved in water-water hydrogen bonds within the single file. Such short hydrogen bonds arise from the presence of an excess proton with its net charge within the proton wire, and are the signature of a proton transferring between water molecules

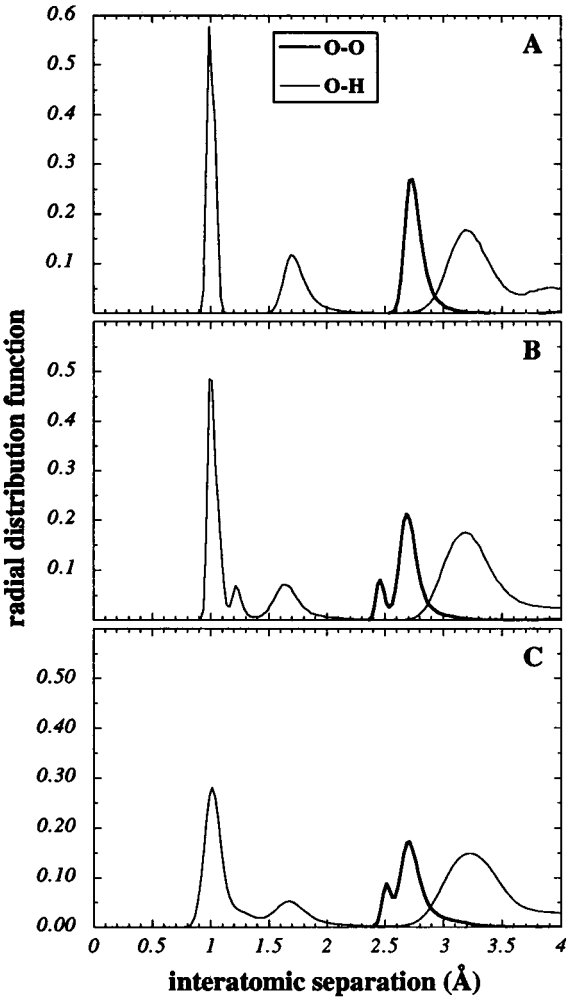

FIGURE 6 Atom-atom radial distribution functions between nearest-neighbor water oxygen atoms (bold) and between water oxygen and hydrogen atoms (thin) in the single-file region of the channel, obtained from simulations A, B, and C. In cases B and C, O-O and O-H densities located, respectively, around 2.5 Å and between 1.2 and 1.3 Å correspond to a short hydrogen bond characteristic of a $O_2H_5^+$-like ion.

(Pomès and Roux, 1995, 1996). It is also consistent with the analysis of the single-file distribution along the channel axis (Fig. 3 *B*). Such hydrogen bonds correspond to the single-well form of the potential energy for the central proton in $O_2H_5^+$, a fundamental feature of proton transfer in strongly hydrogen-bonded systems.

The features observed in Fig. 6 *B* are also present in the quantum case C, although because of the broader distribution of quantum nuclei compared to the classical limit, the "short hydrogen bond" O-H peak does not emerge distinctly from the surrounding covalent and hydrogen-bonding O-H pairs. Furthermore, the short hydrogen bonds are significantly longer than in the classical case B. This arises from the delocalization of the proton in the central energy well of $O_2H_5^+$ due to the zero-point vibration (Pomès and Roux, 1995, 1996). Additionally, broader O-O main peaks in diagrams B and C compared to the unprotonated case A

reflect a distribution of hydrogen bond lengths around the excess proton. Water-water hydrogen bonds tend to become increasingly shorter with increasing proximity to the excess H^+ charge (Pomès and Roux, 1995). The single-file hydrogen bonding structure in case D (not shown) is very similar to case B, although a shorter O-O tail in the 3–4-Å range indicates the absence of weak water-water hydrogen bonds.

Coupling of proton translocation to O-O separation

The above distributions reflect the average geometry of the single-file water chain. We have seen that the presence of an excess proton induces a short hydrogen bond in which the proton is shared by two water molecules. Moreover, the geometry of the entire chain is affected by the presence of a "solvated H^+" cluster, at least in the sense that hydrogen bonds invert around it, as shown in Figs. 2 and 3. Because a greater spread in water-water hydrogen-bonding distance was observed in simulations B and C with respect to the unprotonated case A, it is of interest to consider the average O-O separations of the single-file water molecules as a function of their position along the channel axis.

This is done in Fig. 7, where O-O "bonds" are numbered from 1 (mouth oxygen to O1) to 11 (O10 to mouth oxygen), and the average O-O separations are calculated separately, from simulations A through D. The presence of a persistent defect in the hydrogen-bonded chain connectivity is evident at position 10 for trajectories A, B, and C. However, whereas in case A the average hydrogen bond lengths inside the channel are very consistent at about 2.75 Å, the protonation of the single file has two dramatic effects on its average hydrogen-bonding properties in cases B and C. On the one hand, the hydrogen bonds at the center of the chain are shortened increasingly with their proximity to bond number 5 linking O4 and O5, a location that was observed in Fig. 3 to be the preferred site for a shared proton. On the other hand, the tightened core of the chain induced by the necessity to solvate the net H^+ charge resulted in longer O-O separations near the mouths of the GA channel (bonds 1, 2, and 10, 11).

From the discreteness of atomic water-water distributions (Fig. 6, *B* and *C*), we know that there are two distinct types of water-water hydrogen bonds: the regular kind near 2.75 Å illustrated in case A, and the short kind present in the protonated cases, at around 2.45 Å (classical treatment) or 2.52 Å (quantum treatment). We note that, with an average separation below 2.60 Å, the hydrogen bond number 5 can be expected to be of the short, proton-sharing kind, in roughly half of the configurations sampled in B and C, whereas neighboring hydrogen bonds involving water molecules number 3 through 7 may also be short in a significant fraction of the total number of configurations. Finally, in case D the short average hydrogen bonds among single-file waters arise from both the absence of weak links in the chain and a more uniform distribution of the strong, proton-sharing hydrogen bonds along the wire. In the following, the importance of quantum effects is investigated in greater detail.

Importance of quantum effects

The dispersion of a ring polymer in the Feynman path integral treatment reflects the mean force imposed on a quantum particle (Chandler, 1990). The radii of gyration of two protons involved in water-water hydrogen bonding were calculated. The first of these is the proton between O4 and O5 in hydrogen bond 5, statistically the shortest one along the water chain in 44.8% of the configurations spanned in trajectory C, and the second lies between O8 and O9 in hydrogen bond 8, which was never the shortest in simulation C. The average radius of gyration for the corresponding ring polymers is 0.137 Å and 0.147 Å, respectively. The distribution of the radius of gyration is shown in Fig. 8. These results indicate that the effective potential of

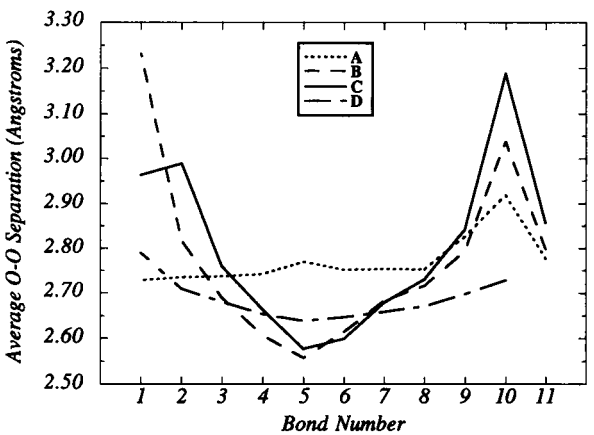

FIGURE 7 Average O-O separations between consecutive water molecules in the single-file region of the channel, obtained from simulations A through D. The preferred locations of H^+ along the single file are marked by a decrease in average O-O separations.

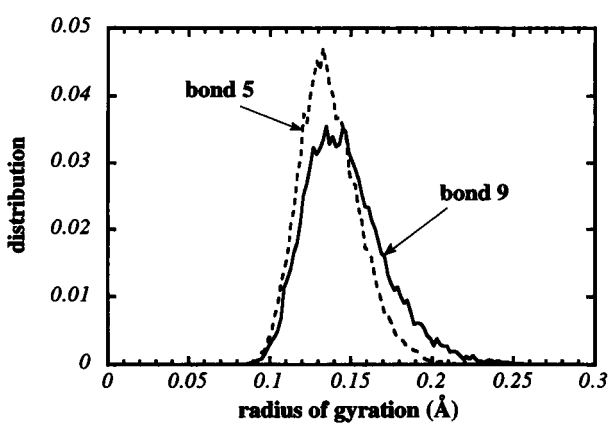

FIGURE 8 Distribution of the radius of gyration of the ring polymers from hydrogen bonds 5 (dashed) and 9 (plain), respectively (trajectory C).

mean force for the motion of protons is very different as their position varies along the water chain.

Comparison with results obtained for a harmonic oscillator helps in appreciating that difference, as well as the magnitude of quantum effects. In contrast with the present system, the dispersion and the fluctuations of a quantum particle in a three-dimensional harmonic potential well can be calculated analytically. Quadratic fluctuations in the position of a classical particle in real time are given by $\langle r^2\rangle_{cl} = 3k_BT/k$, where k is the harmonic force constant shaping the local potential well. The quantum dispersion of a particle with mass m in that well is obtained from

$$\langle r^2\rangle_{qm} = \langle r^2\rangle_{cl}\left(\frac{1}{2}\frac{\hbar}{k_BT}\sqrt{k/m}\right)\coth\left(\frac{1}{2}\frac{\hbar}{k_BT}\sqrt{k/m}\right). \quad (9)$$

In the zero-point energy approximation, valid as long as the vibrational excitation energy $\hbar\omega = \hbar\sqrt{k/m}$ is much larger than the thermal energy k_BT, the dispersion is $3/2\hbar/\sqrt{mk}$.

These quantities, calculated with $T = 300$K and $m = 1$ amu, are shown in Fig. 9 as a function of the harmonic force constant k. The classical limit seriously underestimates the accessible configurational space at all but small values of k. Conversely, the zero point approximation gives a good estimate of the spatial dispersion for $k \geq 150$ kcal/mol/Å^2. In the harmonic approximation, the values of 0.137 and 0.147 Å obtained for the dispersion of the two protons H_a and H_b considered above would correspond to $k = 620$ kcal/mol/Å^2 and $k = 470$ kcal/mol/Å^2, respectively. These two values differ significantly and support the implication that the effective force acting on a proton transferring along a short hydrogen bond is generally greater than that acting on a hydrogen atom in a "regular" hydrogen bond (Pomès and Roux, 1995).

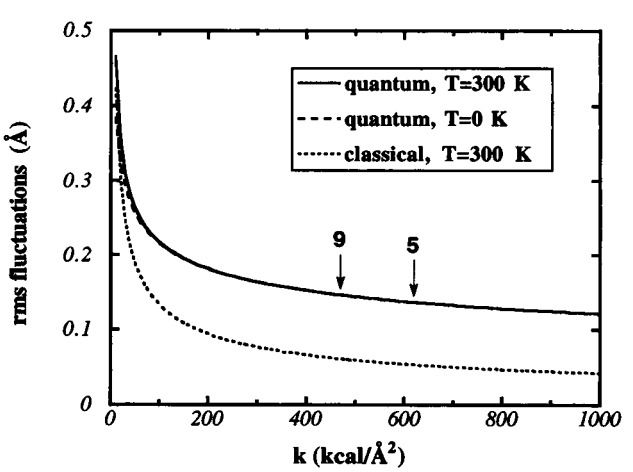

FIGURE 9 Analytical values of the rms fluctuation obtained, respectively, in the full quantum treatment (plain), a quantum treatment including only the zero-point energy (dashed), and in the classical limit (dotted) for a particle in a three-dimensional harmonic well, as a function of the well's force constant k (see text). Arrows indicate the values corresponding to the average dispersion of the Feynman path integral ring polymers of hydrogen bonds 5 and 9 obtained from simulation C.

There are thus significant differences in the geometry of the classical and quantum proton wires, as revealed by the structure of water-water hydrogen bonds in the present study. On average, these hydrogen bonds are longer in the quantum case than in the classical limit. Inclusion of the zero-point energy alone causes significant changes in the configurational space accessible in a simulation, an effect that occurs in the geometry of the chain as the quantum protons resist the increase in localization and compression in a short hydrogen bond. In addition, the strong overlap of the two water oxygen-oxygen peaks in Fig. 6 *C* is such that the distinction between "short" and "standard" hydrogen bonds is not as straightforward as in the classical limit, where the corresponding peaks are well separated. The absence of a well-defined peak in the O-O distribution suggests that a continuum of configurations is accessible. Thus, the transition between long and short hydrogen bond lengths is thermodynamically favored compared to the classical limit, resulting in a greater ease for proton translocation along adjacent hydrogen bonds of the proton wire. Indeed, results obtained from a separate study of water proton wires in vacuo showed that the free energy barriers controlling the interconversion of short hydrogen bond distances along the linear chain of water molecules are significantly lower in the quantum treatment than in the classical limit (Pomès and Roux, 1996). Because the discretized Feynman path integral approach taken here does not make it possible to follow the dynamics of the quantum system, one is left to speculate, in view of the present study, that H^+ translocation along the proton wire could take place more readily than in the classical limit. The question of proton mobility and the extent and dynamics of the translocation are addressed in the remainder of this section.

Choice of a translocation coordinate

The structural results presented so far indicate that there is a strong coupling of the geometry of the single-file water chain with what may be called a "transferring proton." Consequently, the geometry of the hydrogen-bonded water chain may be used to define, characterize and follow the coordinate of proton translocation (Pomès and Roux, 1996). To do so, one may have to make assumptions concerning the nature of the "solvated proton" species. As suggested in Fig. 2, the excess H^+ may take part in a hydronium ion OH_3^+, but it could also induce the formation of $O_2H_5^+$, $O_3H_7^+$, or, in principle, any linear $O_nH_{2n+1}^+$ cluster that fits within the hydrogen-bonded segment of the single-file water chain. To evaluate the choice of a coordinate for H^+ translocation, two candidates were selected and followed for simulation B. The first coordinate is the position of the "hydronium ion." More specifically, the instantaneous location of the oxygen atom nearest to three hydrogen nuclei in a given configuration was singled out from trajectories B and C. The second coordinate is the midpoint of the shortest O-O separation for any given configuration and will be

referred to as "shortest O-O separation." This second choice is equivalent to following the position of the center of transient $O_2H_5^+$ clusters along the channel axis, a reasonable approximation to the position of the proton transferring along a hydrogen bond. This view is justified by the presence, at virtually any point in the trajectory, of one short hydrogen bond induced by the excess proton in which the intervening proton is shared by two oxygen atoms.

The top of Fig. 10 shows histograms for the distribution of the hydronium and shortest O-O coordinates along the channel axis z obtained from simulation B. Each of these two distributions breaks down into a number of distinct peaks. The peaks of the two distributions alternate and appear to reflect complementary views of the translocation, with, respectively, four peaks for the hydronium coordinate intercalated between five short-O-O peaks. The translocation covers as much as 10 Å along the channel axis, or about half of the single-file region. The relative occupancy of shortest O-O peaks is shown in Fig. 10 *B* and confirms the preferred location of the translocating proton near $z = -2$ Å, during our simulations, consistent with observations made earlier. By going beyond the statistical picture, one may gain a better picture of the translocation coordinate. For example, the bimodal H_3O^+ peak at $z \simeq -3.5$ Å underlines a limited translation of the oxygen atom 4 along the channel axis upon sharing a proton alternately with O3 and O5. A closer look at the detailed water-water and water-channel structures underlying each of the discrete translocation states is required to understand the local factors leading to H^+ translocation.

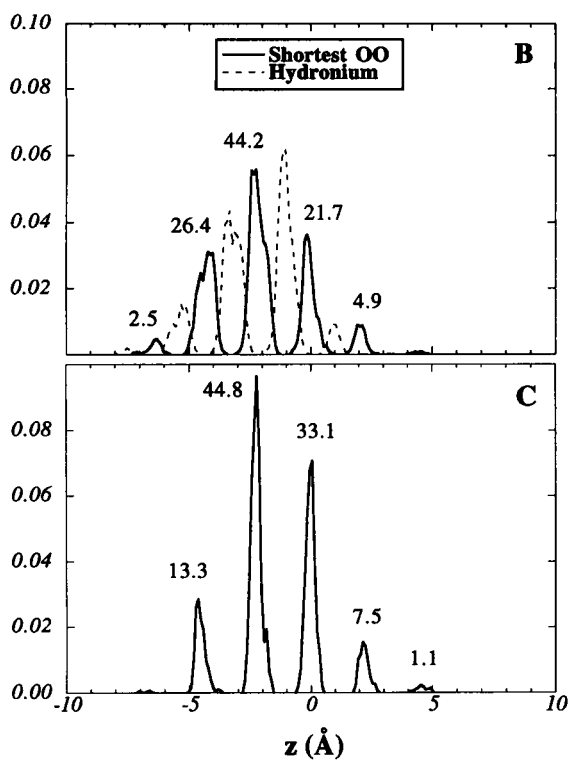

FIGURE 10 Histograms for the distribution of the hydronium oxygen (dashed) and shortest O-O (bold) coordinates along the channel axis z obtained from simulations B (*top*) and C (*bottom*). The relative occurrence of each shortest O-O peak is indicated as a percentage.

The preceding analysis shows that the two proposed reaction coordinates provide equivalent statistical descriptions of the proton mobility in the channel. In a configuration generated by a quantum/classical simulation, the unambiguous determination of OH_3^+ is difficult because protons in a short hydrogen bond are in general shared by two water molecules. In this case, a reaction coordinate involving only heavy atoms is easier to follow. For this reason, only the distribution of the "shortest O-O" coordinate in the quantum case (C) is shown at the bottom of Fig. 10. As in the classical trajectory B, proton translocation spans about 10 Å over the course of the simulation. The distribution of the "transient $O_2H_5^+$ cluster" coordinate is shifted by about 2 Å toward the center of the channel, resulting in a topographically symmetric distribution around the channel junction at $z = 0$. The envelope of the five peaks making up the distribution is asymmetric, and the highest probability of finding a shared proton lies on either side of O5, consistent with observations made earlier from O and H densities along the channel axis. It is interesting to note that this asymmetry, as in the classical trajectory (B), results from the asymmetry in the single-file water distribution in the channel, which is most notable at the end points with the persistent defect in the hydrogen-bonded chain at O9–O10; in turn, this results from the insufficient length of the simulations. However, the significant difference in the overall distribution of the proton translocation coordinate in the quantum case C compared to the classical limit B also stems from important differences in the properties of the water chain due to the quantization of the energy of the protons. This is because the effective potential for the motion of protons is affected by the inclusion of quantum effects (recall Fig. 6 *C*).

Dynamics of the proton wire

So far, only average properties of the proton wire have been considered. The remainder of the Results section is dedicated to the time evolution of the two proton translocation coordinates proposed in the preceding subsection, in relation to the structure and dynamics of the entire chain of water molecules. Figs. 11 and 12 depict the time evolution of the z coordinate of all water oxygen atoms in classical simulations A and B, respectively. In the unprotonated case A (Fig. 11), there is no net diffusion of water molecules inside or outside the channel within the 200 ps of trajectory A; instead, each single-file oxygen atom along the channel axis fluctuates around a generally well-defined position. These features are to be compared to the time-averaged distribution of oxygen atoms in Fig. 3 *A*. At 8.5 Å $\leq z \leq$ 10.5 Å, the defect in hydrogen bonding between O9 and O10 results in a relatively low mobility of O9 due to a comparatively favored hydrogen bonding with carbonyl ox-

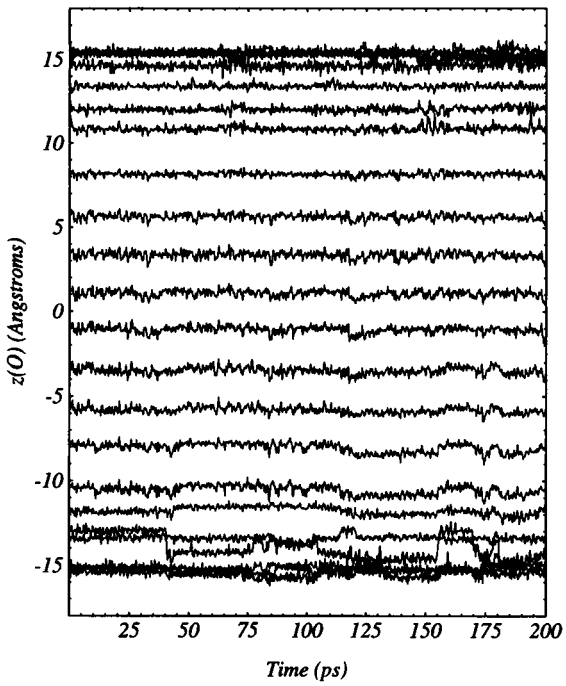

FIGURE 11 Time evolution of the z coordinate of all water oxygen atoms from simulation A. Note the presence of correlated motions.

ygen atoms of the channel backbone. As one moves down the single-file region, the water chain becomes increasingly mobile, and there is a marked collective character to the fluctuations in oxygen positions along the channel axis.

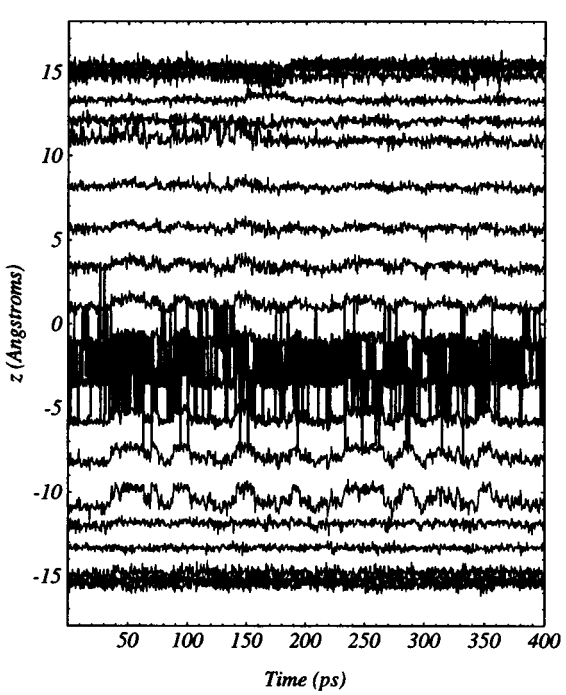

FIGURE 12 Time evolution of the z coordinate of all water oxygen atoms (plain) and of the hydronium oxygen coordinate (bold) from simulation B.

Strong correlations in the dynamics of the single-file water chain were also noted and studied by other authors (Chiu et al., 1991, 1993). In this simulation, the magnitude of correlated motions culminates with water 1, which appears to oscillate between two favored channel positions near $z \simeq -10.5$ Å.

Fig. 12 shows analogous time series obtained from the protonated classical wire of simulation B, with the addition (in bold) of the oxygen of the OH_3^+ coordinate defined in the previous section. Over the course of the simulation, the proton translocation coordinate hopped many times between water molecules within -7.5 Å $\leq z \leq 3.5$ Å, with preferred residence in the -6 Å $\leq z \leq -1$ Å region, as noted before from Fig. 10 *B*. As much as is visible from this graph, the lifetime of transient H_3O^+ ionic species appears to be comparable to the rapid fluctuations of the water molecules in the channel. First, we note that the two water molecules at $z \simeq \pm 12$ Å are less mobile than their single-file counterparts, which reflects the fact that they form hydrogen bonds both with the channel mouths and with the solvent caps, the motions of which are restrained. Overall, the magnitude of fluctuations in the positions of water oxygen atoms in the protonated single file (Fig. 12) is comparable to that observed in the unprotonated case (Fig. 11). Again, the relative mobility of water molecules increases as z decreases, a tendency that culminates in the cases of O1, O2, and O3, respectively, at $z \simeq -10$ Å, $z \simeq -8$ Å, and $z \simeq -5.5$ Å. Each of these three atoms underwent a relatively large displacement of about 1 Å between two preferential positions along the z axis. These displacements appear to be correlated with occasional displacements of the "hydronium coordinate" to water oxygen atoms O2 and O3. The increasing mobility of oxygen atoms with diminishing z arises from the combined effects of hydrogen bond defects near the ends of the single file with opposite consequences: at the "top" of the channel, the defect induces restrictions in the displacement of O9, whereas at the "bottom" of the channel, the defect allows O1 to alternately bind two sites in the channel. The larger flexibility that results near the bottom of the proton wire, in turn, might help to explain the preferred presence of the excess proton in the lower region of the channel. This consideration implies a strong coupling of the proton translocation to the dynamics of the proton wire, which is now considered in more detail.

Fig. 13 shows the water oxygen and hydronium z coordinates over a smaller, 25-ps window in simulation B. That time range is sufficiently short that individual translocations between adjacent single-file oxygen atoms can be distinguished, yet is long enough for a number of representative features to be observed. Most of the time, the proton translocation coordinate is either fluctuating very rapidly between two adjacent water molecules (e.g., at 76 ps $\leq t \leq$ 78 ps, 82 ps $\leq t \leq$ 84 ps) or between three adjacent water molecules (e.g., 90 ps $\leq t \leq$ 94 ps), or is stabilized in a particular H_3O^+-like ion for periods of up to 1 or 2 ps (e.g., 78 ps $\leq t \leq$ 80 ps). Occasionally, H^+ translocation occurs very rapidly over as many as six oxygen atoms (see 88 ps $\leq$

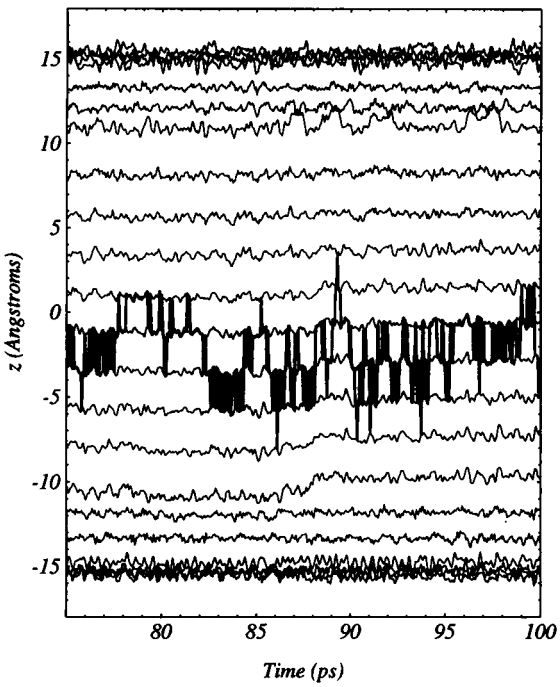

FIGURE 13 Same as Fig. 12 for a shorter time window.

$t \leq 90$ ps), with very short-lived intermediates. From Fig. 13, proton translocation is clearly seen to occur on the time scale of small fluctuations in the position of oxygen atoms along the channel axis. Furthermore, although some cooperativity in the position of oxygen atoms is evident, it does not consist in concerted, collective fluctuations of the single-file water molecules, contrary to the unprotonated chain. A detailed understanding of the coupling of H^+ translocation to the dynamics of other atoms in the proton wire as a whole, consequently, necessitates a closer look at the dynamics and fluctuations in O-O separations along the chain.

The equivalence of the time evolution of the two H^+ translocation coordinates defined earlier, i.e., the "hydronium O" and "shortest O-O" coordinates, can be assessed from Fig. 14 for the 75–100-ps window in the time series of trajectory B. The z coordinate of the midpoint of the shortest O-O separation is shown in bold, and that of the hydronium oxygen atom in dashed lines. The two coordinates follow each other very closely over the 25-ps window considered here. At times, the "short O-O" coordinate appears to fluctuate less than its hydronium counterpart (e.g., at 76 ps $\leq t \leq$ 77.5 ps and 82 ps $\leq t \leq$ 84 ps), which suggests that at these times the protonated species may look more like a $O_2H_5^+$ ion than like H_3O^+. Generally, the two coordinates are within half a hydrogen bond of each other, although discrepancies can occur transiently (e.g., at $t \simeq 78.5$ ps or $t \simeq 90.3$ ps), indicating that neither of them is totally foolproof whenever the geometry of the chain is intermediate between well-defined states. At most times, however, the two coordinates appear to be equally valid depictions of the H^+ translocation coordinate, a result that is reflected in the equivalence of the two distributions of Fig. 10 *B*. Because of the strong coupling between O-O separations and H^+ translocation, it is appropriate to study the dynamics of fluctuations in O-O separations along the single file.

This is done in Fig. 15, where the successive O-O sepa-

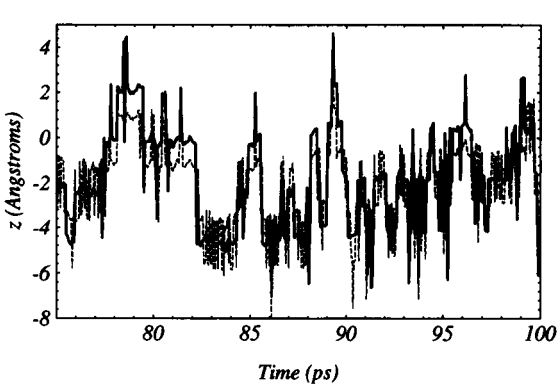

FIGURE 14 Time evolution of the hydronium oxygen (dashed) and shortest O-O (bold) coordinates from simulation B. The time window is the same as in Fig. 13.

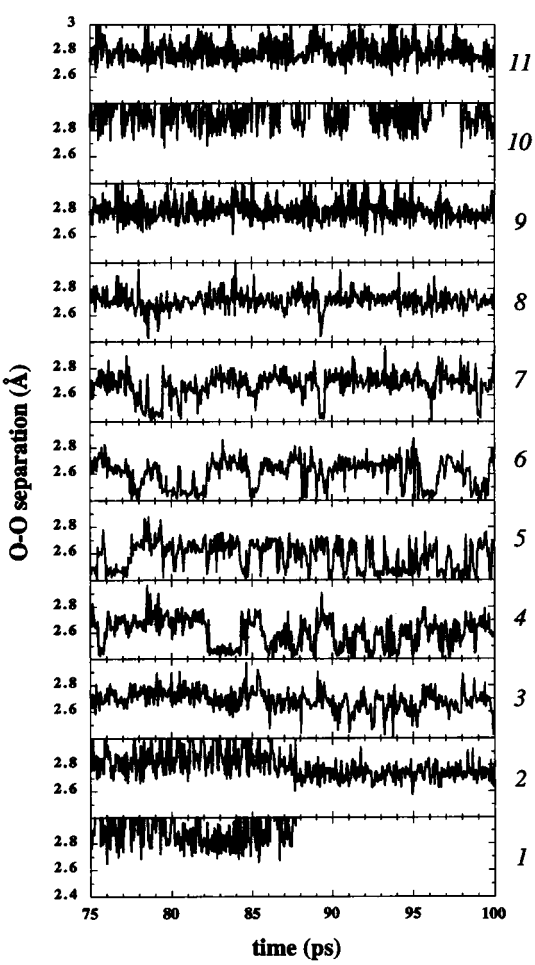

FIGURE 15 Time evolution of all water-water hydrogen bond lengths in the proton wire obtained from simulation B. Bond numbers appear at the right of the figure. The time window is the same as in Fig. 13.

rations in the single-file region are shown as a function of time for the same window in time as in Figs. 13 and 14. As before, O-O separations labeled 1, 2 through 11 correspond to distances between the water at the mouth of the channel and O1, O1 and O2, etc. . . . through the O10-mouth water separation. The O-O distances fall into three categories: 1) intermittent or defectuous (1 and 10), 2) regular (2, 9, and 11), and 3) those alternatively strong and regular (3 through 8); in the latter category, there is a core of four hydrogen bonds that are often short (4 through 7), whereas the outer two are short and strong very occasionally, and then merely in a transient way (3 and 8).

In the "core" of four hydrogen bonds in which the proton is often shared, there are clearly two distinct states corresponding to long and short hydrogen bonds, respectively, at 2.7 Å and 2.45 Å separations. A close look reveals that there is exactly one short hydrogen bond in the proton wire at a given time. Following the propagation of the "shortest O-O" reaction coordinate yields information on the mechanism of H^+ translocation in the proton wire. At $t = 75$ ps, hydrogen bond number 5 is short for about 0.3 ps, then there is a large fluctuation of about 0.2 Å that is anticorrelated with an inverse fluctuation in bond 4, which thereafter becomes short and stays so for about a third of a picosecond; then there is a large fluctuation in the O-O separation that is anticorrelated to bond 5. The latter remains short for about 1.5 ps, and the translocation coordinate then hops successively to bonds 6, 7, 6, 7, 8, 7, etc. . . . , in the manner best depicted in Fig. 14. It is important to note that the successive hops always take place through successive vibrations in the O-O distance of generally adjacent hydrogen bonds. A corollary is that the lifetime of a short O-O bond is limited by thermal fluctuations in the proton wire, and ranges from transient lifetimes of under 0.05 ps to stable ones lasting up to a couple of picoseconds (see bond 4 at 82 ps $\leq t \leq$ 84 ps). Another consequence is that whenever the arrangement of oxygen atoms in the single-file water chain allows it, there are rapid cascades of translocations occurring in a coherent fashion over up to five or six hydrogen bonds, e.g., at 88 ps $\leq t \leq$ 90 ps between bonds 3 and 8.

As one moves up and down along the hydrogen-bonded chain, away from the translocation coordinate, the fluctuations in O-O separations become less influenced by the dynamics of proton translocation. The proximity to the short O-O bond means shorter O-O distances on average (recall Fig. 7), and the transient formation of a tight cluster of water molecules around the excess proton often means a looser connectivity between water molecules a few Å away in the single file, as seen in Fig. 15 for bond 4 at $t \simeq 79$ ps. In the regions never or seldom visited by the translocation coordinate, water-water hydrogen bonds are looser on average and, at the extremities of the single file, they may even be broken. Thus, in Fig. 15 hydrogen bonds labeled 3 and 8 are seldom strong, bonds 2 and 9 are moderately good, whereas bonds 1 and 10 are intermittent. At sufficiently long distances from the net proton charge, the electrostatic forces that pull the water chain together nearer the excess charge are supplanted by the need for water molecules to form good hydrogen bonds with the channel backbone. Near the channel mouth, the mobility of the single-file water molecules is affected by the reduced number of configurations that they can assume to form good hydrogen bonds with a reduced number of peptide bonds. In addition, the mobility of water molecules at the mouth is further limited by the greater accessibility of peptide groups in the last turn of the gramicidin monomer. Conversely, the reduced mobility of the water molecules near the mouths of the channel hinders their full participation in the long-range cooperative thermal motions that help determine the position of the translocation coordinate. The case of bond number 1 at the "bottom" of the single file offers a good illustration (Fig. 15). Both bonds 1 and 2 are intermittent up to $t = 88$ ps, a situation reflected by the distribution of O1 alternatively near the mouth water molecule and near O2. At $t = 88$ ps, bond 1 is suddenly broken, so that bond 2 becomes stronger. Because of the enhanced connectivity and cooperativity at the bottom of the single file, the proton translocation coordinate, which had been confined to regions further up, is then able to visit neighboring hydrogen bond 3 several times in the ensuing 12 ps.

Mechanism of proton translocation

The mechanism of proton translocation along a linear hydrogen-bonded chain has been conceptualized in terms of hopping and turning defects, primarily by Nagle and other workers (Nagle and Morowitz, 1978; Knapp et al., 1980; Nagle and Tristam-Nagle, 1983; Nagle, 1987), based on the theory of proton translocation in ice crystals. Before we consider how the results of this study compare to that model, we briefly review the hop-and-turn mechanism here. Assuming an oriented chain (Scheme 1) in which all hydrogen atoms involved in water-water hydrogen bonds are bound to the oxygen atoms on their left (I), the net translocation of a proton from left to right occurs through successive hypothetical "hops" which, once the proton has exited the chain from the right, leave the chain in an inverted donor-acceptor pattern, with hydrogen atoms binding the oxygen atom to their right (III). This chain reaction has been called diffusion of an "ionic defect" (Nagle and Morowitz, 1978). The passage of another proton down the chain from left to right requires the preliminary inversion of the donor-acceptor pattern in each of the hydrogen bonds in the single file. This second chain reaction, which requires the sequential reorientation (or "turn") of each water molecule, has been described in terms of propagation of a "bonding defect." It is important to note after other authors (Nagle and Morowitz, 1978; Nagle, 1987; Deamer, 1987) that in those channels which mediate the successive translocation of several protons, both stages (hop and turn) are needed for the net translocation of each successive H^+ by the proton wire. Accordingly, each of the hop-and-turn chain reactions can be viewed as the translocation of a

partial charge, corresponding, respectively, to the ionic defect and the bonding defect (Nagle and Morowitz, 1978).

In the gramicidin channel, the proton translocation does not take place through a hypothetical, totally concerted mechanism in which all hydrogen-bonding protons of the chain would hop in a single step. But it does not happen either via a succession of incoherent hops between well-defined hydronium ion intermediates. Rather, proton transfer in the wire is a semidelocalized process that results from the complex interplay of rapid hydrogen-bond length fluctuations along the chain. For lack of a more precise description of the translocation coordinate, the species hosting the excess proton may be described as $O_nH_{2n+1}^+$, a protonated cluster of n single-file water molecules forming a tightly hydrogen-bonded chain within which correlated motions are strong. The nature of this cluster is transient, with n and the precise location of the transferring proton near the cluster's center both varying with rapid thermal fluctuations, and with more infrequent events involving hydrogen bond reorganizations with the channel backbone. This cluster may be identified with the tight "core" described in the analysis of the dynamics of the single file, with $2 \leq n \leq 5$.

The dynamics of important cooperative effects within the single file, like the dynamics of the hydrogen-bonded chain, can be decomposed into two groups. On the one hand, motions occurring in the short-time range ($t \leq 1$ ps) include the rapid fluctuations involving H^+ motions within the tight protonated chain of n water molecules. Hopping of the translocation coordinate occurs through anticorrelated fluctuations in the length of adjacent hydrogen bonds (short/long–long/short isomerization). The cooperativity decreases for O-O bonds lying further away because of decreasing electrostatic interactions along the single file. Importantly, the translocation of proton along the single file does not require large motions of the water molecules. Indeed, fluctuations of 0.2 Å in O-O separations suffice to displace the proton coordinate by about 2 Å along the channel axis. Thus, over short periods of time (on the order of 1 ps), translocation can occur over large portions of the channel without net translation of the water molecules in the single-file region.

On the other hand, the dynamics of water molecules in outlying regions of the single file that are relevant to proton translocation reflect the influence of the channel more directly. Whereas the excess proton is tightly solvated by water molecules in a linear $O_nH_{2n+1}^+$ cluster, the dynamics of water molecules further removed in the single file is less sensitive to electrostatic forces arising from the net charge, and is modulated instead by a delicate balance of hydrogen-bonding interactions with other water molecules and with the channel. Thus, the importance of the balance between water-water and water-channel interactions, noted in previous investigations of ion transport through gramicidin (see Roux and Karplus, 1994, and references therein), appears to be particularly relevant in the case of proton translocation. Occasional exchange between these hydrogen bonds occurs on time scales much longer than fluctuations in O-O distances in the tight protonated cluster, because it is linked perhaps to slow conformational fluctuations in the backbone of the channel dimer, and certainly to the unfrequent, thermally activated net translation of water molecules in the channel. Such motions lead to local reorganizations in the hydrogen-bonding network involving the single-file region of the proton wire, and they occur much less frequently than those governing proton translocation within the protonated cluster. Indeed, the dynamical interconversion that accompanies the making and breaking of a hydrogen bond between water 1 and the water molecule at the mouth of the channel typically occurred every 25 ps or so in trajectory B (see the frequency of 1-Å translations of O1 in Fig. 12). Furthermore, no significant change in the relative strength of the hydrogen bonds involving water 9, another site of disruption in the hydrogen-bonded chain, was evident from the analysis of the entire 400-ps simulation. Yet such modulations in the connectivity of the single file appear to limit the extent of H^+ translocation, as seen in the case of water 1, where the formation of the O1–O2 hydrogen bond correlated with the sharing of a proton by O2 and O3. Inversely, the lack of a good hydrogen bond between O9 and O10 and the subsequent restraints on the dynamics of water molecules at the top of the hydrogen-bonded chain is probably the reason why the proton translocation does not reach the top of the channel over the course of simulation B. The long time scale involved in the reorganization of the hydrogen bonds in the single file is notably consistent with the very slow diffusion of waters inside the channel; as seen from Table 1, the diffusion of waters inside the GA channel is reduced by a factor of 50 compared to the bulk. In effect, the relative mobility of water molecules and H^+ differs more markedly inside the channel than in the bulk.

To summarize the above analysis, it appears that the cooperativity among water molecules, which facilitates a rapid translocation in the single file, is affected by limits in the flexibility of the linear water chain imposed by hydrogen bonding with the channel. Whereas the competition is not significant at the center of the channel, where H^+ translocation is fast, it is sufficient to reduce the cooperativity between water motions near the mouths of the GA channel, so that the dynamics of H^+ translocation, ultimately, is limited by the dynamics of bonding "defects" in the connectivity of the proton wire. In the present system, as in ice (Nagle and Morowitz, 1978), propagation of an ionic defect appears to occur on a time scale at least one order of magnitude shorter than that of bonding defects. This is in qualitative agreement with the conclusions reached by Akeson and Deamer (1991) in an extensive experimental study of the GA conductance to proton.

The last result presented here illustrates the importance of the bonding defect on the dynamics of H^+ translocation in the GA channel. Fig. 16 depicts the time evolution of single-file waters and of the hydronium coordinate along the channel axis computed from the "hydrophobic channel" simulation D, in which the computation of electrostatic interactions between the channel and water atoms was omit-

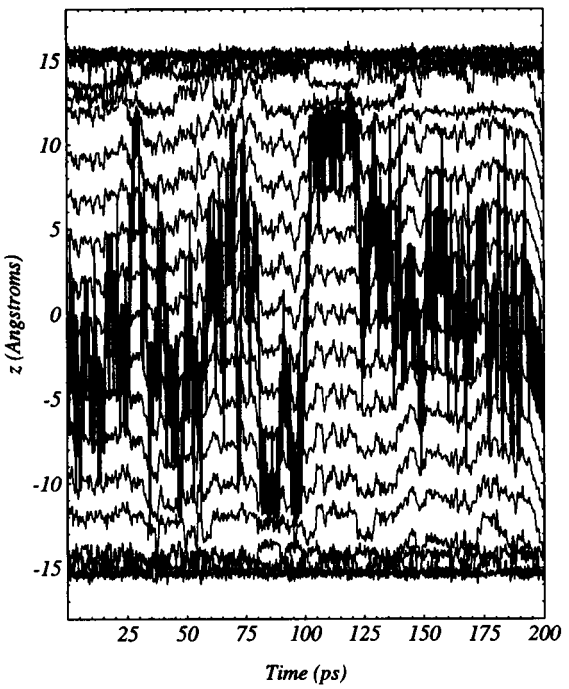

FIGURE 16 Time evolution of the z coordinate of all water oxygen atoms (plain) and of the hydronium oxygen coordinate (bold) from the "hydrophobic channel" simulation D.

ted. These results show a dramatic increase in the mobility of the water molecules and, above all, of the hydronium z coordinate. Because there are no more water-channel hydrogen bonds, there is now no preferred position for the single-file water molecules along the channel axis. Better water-water hydrogen bonds can therefore be formed and maintained, so that the proton wire also displays a very strong cooperativity, with water displacements correlating from end to end. As a consequence, H^+ mobility is strikingly enhanced, with very rapid hops spanning the entire length of the channel within a few picoseconds. In this line of thought, it is interesting to note that the higher proton mobility exhibited by our model "hydrophobic channel" simulation D is consistent with recent experimental observations of very fast proton translocation across lipid bilayers, which was attributed to transient transmembrane channels formed by hydrophobic polyamino acid α-helices (Oliver and Deamer, 1994).

CONCLUSION

In this work we have studied the properties of both unprotonated and protonated linear chains of water molecules in the pore of the gramicidin channel. To our knowledge, this is the first attempt to investigate a proton wire in a biologically relevant system using a molecular model. Whereas the presence of an excess proton in the single file does not affect the conformation of the channel, it strongly influences the geometry of the water wire by inducing a strong hydrogen bond in which the proton is shared by two water molecules. Additionally, the net charge pulls much of the rest of the hydrogen-bonded chain closer together and orients it. The properties of the water chain are also affected by the quantization of the proton motions, with the quantum dispersion of hydrogen nuclei resisting compression in short hydrogen bonds. The atomic distribution functions along the proton wire suggest that the transfer of a proton between hydrogen-bonded water molecules is facilitated by the inclusion of quantum effects. In a previous study of water wires in vacuo, this effect was attributed primarily to the zero-point energy of the protons, and more marginally to tunneling (Pomès and Roux, 1995).

As for the mechanism of the gramicidin proton wire, the transfer was seen to be strongly coupled to the geometry and the dynamics of the water chain. The translocation of a proton between adjacent water molecules in the chain occurs spontaneously, with successive thermal fluctuations of O-O separations. The process does not take place via a totally concerted mechanism in which the donor-acceptor pattern would flip over the entire chain in a single step, nor does it happen via a succession of incoherent hops between well-defined hydronium ion intermediates. Rather, proton transfer in the wire is a semicollective process that results from the subtle interplay of rapid hydrogen-bond-length fluctuations along the water chain. Thus, the proton transfer coordinate hovers back and forth and may travel over several consecutive hydrogen bonds within a few picoseconds. These observations have important implications for constructing theoretical models of proton wires. For instance, it may not be appropriate to describe the rapid dynamics of the ionic defect in terms of an incoherent stochastic Markov rate process (Knapp et al., 1980). On a short time scale, the dynamics of the protonated linear cluster exhibits frequent coherent and strongly correlated microscopic events. In addition, because of the significant delocalization of the protonated cluster, a meaningful theoretical model must allow the transfer to take place over the full extent of the single file of water molecules. This warns against theoretical approaches in which proton dissociation would be taken into account within a pair of water molecules, whereas the other waters in the channel would be treated with a classical nondissociable model.

Importantly, the results obtained from our simulations indicate that hydrogen bonds between single-file waters and the channel stabilize the local structure of the proton wire and thereby diminish the integrity of the hydrogen-bonded water chain. In turn, the properties governing proton transfer along the chain are modified. This is especially notable near the mouths of the channel, where the greater accessibility of the protein backbone allows for a better binding of the water molecules, thus generating defects, or weak links in the water chain, that prevented full H^+ translocation across the channel over the course of our simulations. Moreover, the closing of a defect, or its migration in one direction, causes the excess proton to quickly translocate in the same direction. Based on this study, one may conclude that the full translocation represented in Scheme 1, step II, could

be two orders of magnitude faster than the complete reorientation of the hydrogen-bonded chain of the single-file water molecules necessary to go from structure III to structure I. These observations suggest that the formation and breaking of hydrogen bonds with the channel constitute the limiting factor for the translocation of protons across the membrane.

Despite rapid excursions along the single file of water molecule, the excess proton remains localized on average around $z = -2$ Å, resulting in no net transport over the length of the simulations. This observation should be not interpreted as an indication that a proton binding site exists near the center of the dimer at monomer-monomer junctions. Test simulations in which the proton was equilibrated at different locations along the channel axis demonstrate that a large number of stable positions can be found elsewhere in the system. The rapid structural fluctuations of the protonated single-file of waters around an average position and the slow movements of the average position along the channel axis occur on two very different time scales. Although this is difficult to prove, it appears that the translocation mechanism is controlled by processes involving the slow rearrangement of the complex hydrogen bond network in the system. The significantly increased proton mobility observed in simulation D strongly suggests that water-channel hydrogen bonds are particularly important and determine the rate of transport.

Perhaps a lesson of general importance to proton transfer along chains of water molecules in protein cavities is that proton conductance requires the presence of a well-connected chain of hydrogen bonds. Furthermore, this chain has to be flexible enough to undergo cooperative motions that facilitate the translocation, which occurs via a succession of rapid transfers between nearest water neighbors coupled to the donor-acceptor separation. However, the flexibility of the water chain is to be balanced against the need for interactions with hydrophilic groups that allow the very presence of water in the pore.

These conclusions help delineate future directions for theoretical research. For instance, a quantitative evaluation of the rate limitation may require a more realistic channel mouth environment. Molecular dynamics simulations performed on larger systems that include the lipid bilayer and large solvent caps would make it possible to address important questions, such as the influence of bulk to channel translocation on the mechanism, and perhaps help in the definition of a collective reaction coordinate. In turn, such a parameter would open the way to the calculation of free energy profiles for proton translocation in ways similar to what has been done with other cations (Roux and Karplus, 1994), and could ultimately make possible a quantitative comparison with experimental measurements of conductance through the refinement of kinetic models that take into account the presence of an external field, such as the model proposed by Prokop and Skála (1994). The computational study of proton wires in this and other transmembrane systems should continue to offer useful insight into the mechanisms controlling biological H^+ translocation.

We thank Dr. T. B. Woolf for providing the initial solvated GA structure.

This work was supported by a grant from the Medical Research Council of Canada. BR is a FRSQ research fellow.

REFERENCES

Akeson, M., and D. W. Deamer. 1991. Proton conductance by the gramicidin water wire. *Biophys. J.* 60:101–109.

Allen, M. P., and D. J. Tildesley. 1987. Computer Simulations of Liquids. Clarendon Press, Oxford.

Arseniev, A. S., V. F. Bystrov, T. V. Ivanov, and Y. A. Ovchinnikov. 1985. ^{1}H-NMR study of gramicidin-A transmembrane ion channel. Head-to-head right-handed, single stranded helices. *FEBS Lett.* 186:168–174.

Azzouz, H., and D. Borgis. 1992. A quantum molecular-dynamics study of proton-transfer reactions along asymmetrical hydrogen bonds in solution. *J. Chem. Phys.* 98:7361–7374.

Bala, P., B. Lesyng, and J. A. McCammon. 1994. Applications of quantum-classical and quantum-stochastic molecular dynamics simulations for proton transfer processes. *Chem. Phys.* 180:271–285.

Berendsen, H. J. C., J. P. M. Postma, W. F. van Gunsteren, and J. Hermans. 1981. Interaction models for water in relation to proteins hydration. *In* Intermolecular Forces. B. Pullman, editor. Reidel, Dordrecht. 331–342.

Brooks, B. R., R. E. Bruccoleri, B. D. Olafson, D. J. States, S. Swaminathan, and M. Karplus. 1983. CHARMM: a program for macromolecular energy minimization and dynamics calculations. *J. Comput. Chem.* 4:187–217.

Cao, Y., G. Váró, M. Chang, B. Ni, R. Needleman, and J. K. Lanyi. 1991. Water is required for proton transfer from aspartate-96 to the bacteriorhodopsin Schiff base. *Biochemistry.* 30:10972–10979.

Chandler, D. 1990. Theory of quantum processes in liquids. *In* Les Houches, Session LI, 1989. Liquids, Freezing and Glass Transition. D. Levesque, J. P. Hansen and J. Zinn-Justin, editors. Elsevier, Amsterdam. 1–101.

Chandler, D., and P. G. Wolynes. 1980. Exploiting the isomorphism between quantum theory and classical statistical mechanics of polyatomic fluids. *J. Chem. Phys.* 74:4078–4095.

Cheng, H.-P., R. N. Barnett, and U. Landman. 1995. All-quantum simulations: H_3O^+ and $H_5O_2^+$. *Chem. Phys. Lett.* 237:161–170.

Chiu, S.-W., E. Jakobsson, S. Subramaniam, and J. A. McCammon. 1991. Time-correlation analysis of simulated water motion in flexible and rigid gramicidin channels. *Biophys. J.* 60:273–285.

Chiu, S.-W., J. A. Novotny, and E. Jakobsson. 1993. The nature of ion and water barrier crossings in a simulated ion channel. *Biophys. J.* 64: 98–108.

Chiu, S.-W., S. Subramaniam, E. Jakobsson, and J. A. McCammon. 1989. Water and polypeptide conformations in the gramicidin channel. A molecular dynamics study. *Biophys. J.* 56:253–261.

Deamer, D. W. 1987. Proton permeation of lipid bilayers. *J. Bioenerg. Biomembr.* 19:457–479.

Del Bene, J. E. 1988. Ab initio molecular orbital study of the structures and energies of neutral and charged bimolecular complexes of H_2O with the hydrides AH_n (A=N, O, F, P, S, and Cl). *J. Phys. Chem.* 92:2874–2880.

Etchebest, C., and A. Pullman. 1986a. The gramicidin A channel: energetics and structural characteristics of the progression of a sodium ion in the presence of water. *J. Biomol. Struct. Dyn.* 3:805–825.

Etchebest, C., and A. Pullman. 1986b. The gramicidin-A channel—the energy profile calculated for Na^+ in the presence of water with inclusion of the flexibility of the ethanolamine tail. *FEBS Lett.* 204:261–265.

Feynman, R. P., and A. R. Hibbs. 1965. Quantum Mechanics and Path Integrals. McGraw-Hill, New York.

Field, M. J., P. A. Bash, and M. Karplus. 1990. A combined quantum mechanical and molecular mechanical potential for molecular dynamics simulations. *J. Comp. Chem.* 11:700–733.

Finkelstein, A., and O. S. Andersen. 1981. The gramicidin A channel: a review of its permeability characteristics with special reference to the single-file aspect of transport. *J. Membr. Biol.* 59:155–171.

Fornili, S. L., D. P. Vercauteren, and E. Clementi. 1984. Water structure in the gramicidin A transmembrane channel. *Biochim. Biophys. Acta.* 771: 151–164.

Gao, J., and X. Xia. 1992. A priori evaluation of aqueous polarization effects through Monte Carlo QM-MM simulations. *Science.* 258: 631–635.

Guo, H., and M. Karplus. 1992. Ab initio studies of hydrogen bonding of *N*-methylacetamide: structure, cooperativity, and internal rotational barriers. *J. Phys. Chem.* 96:7273–7287.

Hille, B. 1992. Ionic Channels of Excitable Membranes. Sinauer Associates, Sunderland, MA.

Hladky, S. B., and D. A. Haydon. 1972. Ion transfer across lipid membranes in the presence of gramicidin A. *Biochim. Biophys. Acta.* 274: 294–312.

Jeng, M.-F., and S. W. Englander. 1991. Stable submolecular folding units in a non-compact form of cytochrome *c*. *J. Mol. Biol.* 221:1045–1061.

Jordan, P. C. 1990. Ion-water and ion-polypeptide correlations in a gramicidin-like channel. *Biophys. J.* 58:1133–1156.

Jorgensen, W. L., J. Chandrasekhar, J. D. Madura, R. W. Impey, and M. L. Klein. 1983. Comparison of simple potential functions for simulating liquid water. *J. Chem. Phys.* 79:926–935.

Ketchem, R. R., W. Hu, and T. A. Cross. 1993. High-resolution conformation of gramicidin A in lipid bilayer by solid-state nmr. *Science.* 261:1457–1460.

Kim, K. S. 1985. Microscopic effect of an applied voltage on the solvated gramicidin A transmembrane channel in the presence of Na^+ and K^+ cations. *J. Comp. Chem.* 6:256–263.

Knapp, E.-W., K. Schulten, and Z. Schulten. 1980. Proton conduction in linear hydrogen-bonded systems. *Chem. Phys.* 46:215–229.

Komatsuzaki, T., and I. Ohmine. 1994. Energetics of proton transfer in liquid water. I. Ab initio study for origin of many-body interaction and potential energy surfaces. *Chem. Phys.* 180:239–269.

Kuharski, R. A., and P. J. Rossky. 1985. A quantum mechanical study of structure in liquid H_2O and D_2O. *J. Chem. Phys.* 82:5164–5177.

Laria, D., G. Ciccotti, M. Ferrario, and R. Kapral. 1994. Activation free energy for proton transfer in solution. *Chem. Phys.* 180:181–189.

Levitt, D. G. 1984. Kinetics of movements in narrow pores. *Curr. Top. Membr. Transp.* 21:181–197.

Lobaugh, J., and G. A. Voth. 1992. Calculation of quantum activation free energies for proton transfer reactions in polar solvents. *Chem. Phys. Lett.* 198:311–315.

MacKay, D. H., P. H. Berens, K. R. Wilson, and A. T. Hagler. 1984. Structure and dynamics of ion transport through gramicidin A. *Biophys. J.* 46:229–248.

MacKay, D. H., and K. R. Wilson. 1986. Possible allosteric significance of water structures in proteins. *J. Biomol. Struct. Dyn.* 4:491–500.

Martinez, S. E., W. A. Cramer, and J. L. Smith. 1995. An internal H_2O chain in cytochrome *f*. *Biophys. J.* 68:A246.

Mavri, J., and H. J. C. Berendsen. 1995. Calculation of the proton transfer rate using density matrix evolution and molecular dynamics simulations—inclusion of the proton excited states. *J. Phys. Chem.* 99: 12711–12717.

Nagle, J. F. 1987. Theory of passive proton conductance in lipid bilayers. *J. Bioenerg. Biomembr.* 19:413–426.

Nagle, J. F., and H. J. Morowitz. 1978. Molecular mechanisms for proton transport in membranes. *Proc. Natl. Acad. Sci. USA.* 75:298–302.

Nagle, J. F., and S. Tristam-Nagle. 1983. Hydrogen bonded chain mechanism for proton conduction and proton pumping. *J. Membr. Biol.* 74:1–14.

Oliver, A. E., and D. W. Deamer. 1994. α Helical hydrophobic polypeptides form proton-selective channels in lipid bilayers. *Biophys. J.* 66: 1364–1379.

Pomès, R., and B. Roux. 1995. Quantum effects on the structure and energy of a protonated linear chain of hydrogen-bonded water molecules. *Chem. Phys. Lett.* 234:416–424.

Pomès, R., and B. Roux. 1996. Theoretical study of H^+ translocation along a model proton wire. *J. Phys. Chem.* 100:2519–2527.

Prokop, P., and L. Skála. 1994. Theory of proton transport along a hydrogen bond chain in an external field. *Chem. Phys. Lett.* 223:279–282.

Pullman, A. 1987. Energy profiles in the gramicidin A channel. *Q. Rev. Biophys.* 20:173–200.

Roux, B. 1995. Theory of transport in ion channels. From molecular dynamics simulations to experiments. *In* Computer Modelling in Molecular Biology. J. M. Goodfellow, editor. VCH, Weinheim, Germany.

Roux, B., and M. Karplus. 1991. Ion transport in a gramicidin-like channel: dynamics and mobility. *J. Phys. Chem.* 95:4856–4868.

Roux, B., and M. Karplus. 1994. Molecular dynamics simulations of the gramicidin channel. *Annu. Rev. Biophys. Biomol. Struct.* 23:731–761.

Scheiner, S. 1985. Theoretical studies of proton transfers. *Acc. Chem. Res.* 18:174–180.

Scheiner, S. 1994. Ab initio studies of hydrogen bonds: the water dimer paradigm. *Annu. Rev. Chem. Phys.* 45:23–56.

Skerra, A., and J. Brickman. 1987. Structure and dynamics of one-dimensional ionic solutions in biological transmembrane channels. *Biophys. J.* 51:969–976.

Stillinger, F. H. 1979. Dynamics and ensemble averages for the polarization models of molecular interactions. *J. Chem. Phys.* 71:1647–1651.

Stillinger, F. H., and C. W. David. 1978. Polarization model for water and its ionic dissociation products. *J. Chem. Phys.* 69:1473–1484.

Urry, D. W. 1971. The gramicidin A transmembrane channel: a proposed π_{LD} helix. *Proc. Natl. Acad. Sci. USA.* 68:672–676.

Weber, T. A., and F. H. Stillinger, 1982. Reactive collisions of H_3O^+ and OH^- studied with the polarization model. *J. Phys. Chem.* 86: 1314–1318.

Woolf, T. B., and B. Roux. 1994. Molecular dynamics simulation of the gramicidin channel in a phospholipid bilayer. *Proc. Natl. Acad. Sci. USA.* 91:11631–11635.

Woolf, T. B., and B. Roux. 1996. Structure, energetics, and dynamics of lipid-protein interactions: a molecular dynamics study of the gramicidin A channel in a DMPC bilayer. *Proteins Struct. Funct. Genet.* 24:92–114.

Wüthrich, K. 1986. NMR of Proteins and Nucleic Acids. John Wiley and Sons, New York.

Zheng, C., C. F. Wong, J. A. McCammon, and P. G. Wolynes. 1989. Classical and quantum aspects of ferrocytochrome *c*. *Chim. Scripta.* 29A:171–179.